NANO · MICRO small
www.small-journal.com

Quinic Acid-Conjugated Nanoparticles Enhance Drug Delivery to Solid Tumors via Interactions with Endothelial Selectins

*Jun Xu, Steve Seung-Young Lee, Howon Seo, Liang Pang, Yearin Jun, Ruo-Yu Zhang, Zhong-Yin Zhang, Pilhan Kim, Wooin Lee, Stephen J. Kron, and Yoon Yeo**

Current nanoparticle (NP) drug carriers mostly depend on the enhanced permeability and retention (EPR) effect for selective drug delivery to solid tumors. However, in the absence of a persistent EPR effect, the peritumoral endothelium can function as an access barrier to tumors and negatively affect the effectiveness of NPs. In recognition of the peritumoral endothelium as a potential barrier in drug delivery to tumors, poly(lactic-co-glycolic acid) (PLGA) NPs are modified with a quinic acid (QA) derivative, synthetic mimic of selectin ligands. QA-decorated NPs (QA-NP) interact with human umbilical vein endothelial cells expressing E-/P-selectins and induce transient increase in endothelial permeability to translocate across the layer. QA-NP reach selectin-upregulated tumors, achieving greater tumor accumulation and paclitaxel (PTX) delivery than polyethylene glycol-decorated NPs (PEG-NP). PTX-loaded QA-NP show greater anticancer efficacy than Taxol or PTX-loaded PEG-NP at the equivalent PTX dose in different animal models and dosing regimens. Repeated dosing of PTX-loaded QA-NP for two weeks results in complete tumor remission in 40–60% of MDA-MB-231 tumor-bearing mice, while those receiving control treatments succumb to death. QA-NP can exploit the interaction with selectin-expressing peritumoral endothelium and deliver anticancer drugs to tumors to a greater extent than the level currently possible with the EPR effect.

1. Introduction

Nanoparticles (NPs) have been considered a promising carrier of chemotherapeutic drugs.[1] The premise of NP-based chemotherapy is based on the notion that tumors tend to develop hypervasculature and poor lymphatic systems and, thus, provide selective access for NPs.[2] This phenomenon, called the enhanced permeability and retention (EPR) effect, has become the governing principle of most NP-based drug delivery. Nevertheless, the utility of NP-based chemotherapy has recently been challenged, due to the low tumor distribution of NPs[3] and the lack of evidence supporting the clinical benefits of NPs.[4] One of the potential reasons that limit NP delivery to tumors is the complex nature of the disease and high intersubject and intrasubject differences, which result in variable efficiency of the EPR effect.[5] For the clinical success of NP-based chemotherapy, there should be additional means

Dr. J. Xu, Prof. Y. Yeo
Department of Industrial and Physical Pharmacy
Purdue University
575 Stadium Mall Drive, West Lafayette, IN 47907, USA
E-mail: yyeo@purdue.edu
Dr. S. S.-Y. Lee, Prof. S. J. Kron
Ludwig Center for Metastasis Research
The University of Chicago
5758 South Maryland Avenue, MC 9006, USA
Dr. S. S.-Y. Lee, Prof. S. J. Kron
Department of Molecular Genetics and Cellular Biology
The University of Chicago
929 East 57th Street, GCIS W519, Chicago, IL 60637, USA
H. Seo, Prof. P. Kim
Graduate School of Nanoscience and Technology and KAIST Institute for Health Science and Technology
Korea Advanced Institute of Science and Technology (KAIST)
291 Daehak-ro, Yuseong-gu, Daejeon 34141, Republic of Korea
The ORCID identification number(s) for the author(s) of this article can be found under https://doi.org/10.1002/smll.201803601.
Dr. L. Pang
Department of Pharmaceutics
School of Pharmacy
Fudan University
Shanghai 201203, P. R. China
Y. Jun, Prof. W. Lee
College of Pharmacy and Research Institute of Pharmaceutical Sciences
Seoul National University
Seoul 08826, Republic of Korea
Dr. R.-Y. Zhang, Prof. Z.-Y. Zhang
Department of Medicinal Chemistry and Molecular Pharmacology
Purdue University
720 Clinic Drive, West Lafayette, IN 47907, USA
Prof. P. Kim
Graduate School of Medical Science and Engineering
KAIST
291 Daehak-ro, Yuseong-gu, Daejeon 34141, Republic of Korea
Prof. Y. Yeo
Weldon School of Biomedical Engineering
Purdue University
West Lafayette, IN 47907, USA

DOI: 10.1002/smll.201803601

to leverage the EPR effect and enhance the delivery efficiency of NPs beyond the level currently possible.

We envision that the vascular endothelium—the first cell layer circulating NPs encounter—serves as an access barrier to the underlying tumors; therefore, NPs that can actively interact with the endothelial barrier will have a greater chance to extravasate into the tumors. In this regard, we note E- and P-selectins, endothelial adhesion molecules expressed in response to local inflammatory stimuli. In the vasculature surrounding inflamed tissues, selectins mediate the interaction of leukocytes with the endothelium and their trafficking into the underlying tissues.[6] In addition to the well-known roles in inflammation, selectins are also implicated in cancer as a mediator of cell adhesion in metastasis and angiogenesis.[7] On the peritumoral endothelium, E-selectin promotes angiogenesis[8] and tumor proliferation[9] and serves as an adhesion point for circulating tumor cells and endothelial progenitor cells to support metastasis.[10] P-selectin is expressed constitutively in endothelial cells and platelets and stored in Weibel–Pallade bodies and α-granules, respectively.[11] Upon activation, P-selectin translocates from the intracellular granules to the cell membrane to mediate the adhesion and activation of leukocytes and platelets.[12] In tumor, P-selectin mediates endothelial interaction with circulating cancer cells as well as their aggregates with platelets.[13] Consistent with their roles in tumor progression, selectins are shown to be overexpressed in various human cancers[14] including breast,[15] kidney,[16] and lung cancers.[17] A recent study reports that among 420 clinical samples examined by immunohistochemistry, selective P-selectin expression is observed in multiple tumor types, including lung (19%), ovarian (68%), lymphoma (78%), and breast (49%) tumors.[14] In addition, selectin expression in tumor can be artificially induced by local ionizing radiation,[12b,18] which is a clinically used cancer treatment protocol. Although the application for patients with other inflammatory diseases may be limited, the prevalent selectin expression in various types of tumor and the potential to induce local selectin expression in tumors suggest that NPs with affinity for selectins may preferentially bind to peritumoral endothelium and afford an increased chance to extravasate into tumors.

One of the natural ligands for selectins is sialyl Lewis-x (sLe^x), an oligosaccharide consisting of fucose, galactose, N-acetyllactosamine, and N-Acetylneuraminic acid.[19] sLe^x and its analogs have been widely explored as selectin antagonists for the therapy of inflammatory diseases[20] and the prevention of metastasis.[21] In particular, quinic acid (QA) and its derivatives have been noted as promising sLe^x mimics due to the ease of chemical modification.[22] These sLe^x mimics have been used as targeting ligands of macromolecular and NP drug carriers for the targeted delivery of chemotherapeutic drugs to the peritumoral endothelium.[14,21b,22b,23] The affinity of QA derivatives for selectins is not high, comparable to sLe^x, with a millimolar range of the half maximal inhibitory concentration (IC_{50}), in the inhibition of P-selectin binding to its natural ligand.[20h] We reason that the weak affinity ligand–receptor interactions may be beneficial for NP delivery to tumors, as they will not prevent the NP transport beyond the endothelial binding. Here, the anticipated role of QA ligand on NP surface is to transiently populate NPs on the peritumoral endothelium, permitting the NPs to extravasate into the tumors.

Ligand-decorated NPs may be produced in various ways. First, NPs can be incubated with functional ligands to allow their physisorption on the NP surface.[24] However, the physisorbed ligands have limited stability in blood, where multiple molecular interactions can interfere with the NP–ligand interactions. Alternatively, ligands may be covalently conjugated to the surface via chemical reactions between functional groups of ligands and NP surface.[25] However, this method requires the presence of reactive functional groups on NPs, which are not always available in a desirable quantity. This leads to an increasingly complex adaptation of NP platforms, such as prefunctionalization of constituent polymers or chemical activation of the NP surface, imposing additional difficulties on the product development. To address this challenge, we employed a simple surface functionalization method based on dopamine polymerization, applicable to a variety of NP platforms irrespective of their chemical reactivity.[26] The dopamine polymerization method involves a simple incubation of NPs with dopamine in an oxidizing condition, which allows dopamine to polymerize and form a chemically reactive layer on the NP surface that accommodates ligand molecules.[27] This method allows for conjugation of various types of ligands, including a QA derivative, and flexible control of QA density on the NP surface. Such versatility and flexibility enable us to investigate the optimal conditions to conjugate QA on NPs for their transendothelial transport and compare the QA-modified NPs (QA-NP) with those containing typical stealth coating such as polyethylene glycol (PEG).

In this study, we demonstrate that QA mediates NP interaction with activated endothelial cells expressing selectins, promotes the NP transport across the activated endothelial layer in vitro, and brings more NPs to tumors than PEG-modified NPs (PEG-NP) in animal models. Consequently, paclitaxel (PTX) loaded in QA-NP (PTX@QA-NP) demonstrates greater anticancer effects than Taxol or PTX loaded in PEG-NP (PTX@PEG-NP) at the equivalent dose in multiple animal models and dosing regimens.

2. Results and Discussion

2.1. Synthesis of QA-NH_2, Synthetic Mimic of sLe^x

QA-NH_2, a synthetic mimic of sLe^x, was synthesized according to the previously reported scheme with slight modification (**Figure 1**a).[23a] The overall yield was 62%. ^{1}H NMR confirmed the structure of the compound (Figure S1, Supporting Information). Electron spray ionization mass spectrometry (ESI-MS) found the mass to charge (m/z) ratio of the compound to be 324.9 (negative ionization mode) as expected (Figure S2, Supporting Information). QA-NH_2 had no adverse effects on human umbilical vein endothelial cells (HUVEC) proliferation (Figure S3, Supporting Information).

2.2. Development and Characterization of QA-NP

QA-NP was prepared with the dopamine-mediated surface modification method.[26] PLGA NPs (bare NP) were first

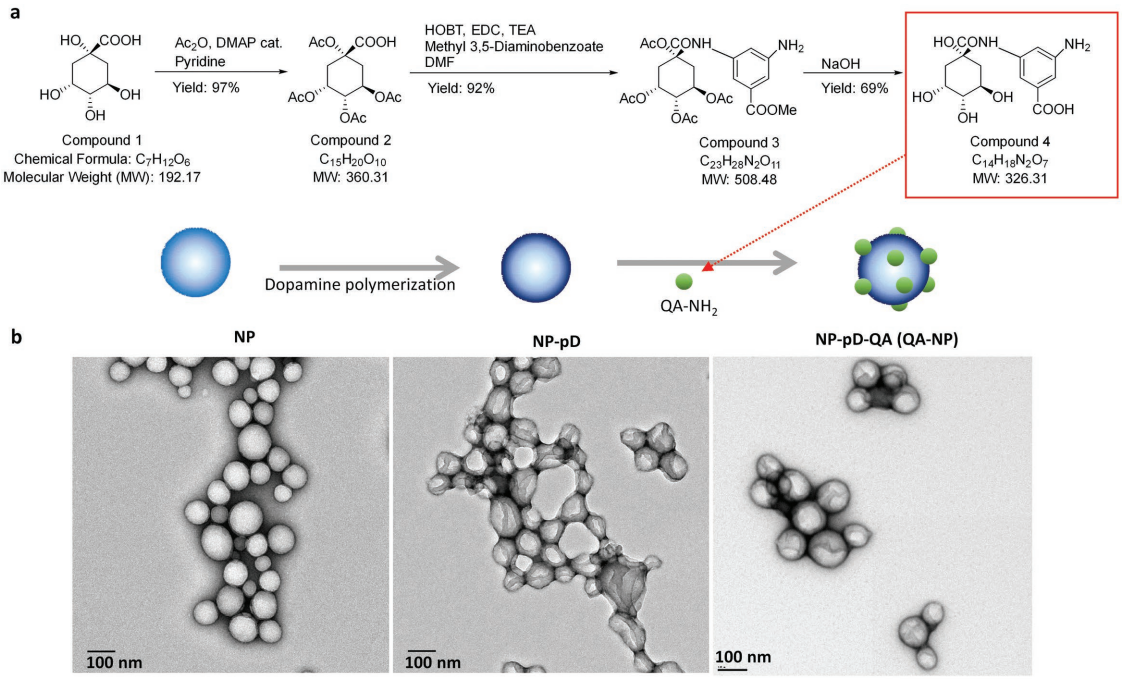

Figure 1. a) Schematic of a quinic acid derivative, QA-NH_2, a synthetic mimic of sLe^x. Overall yield: 62%. b) Transmission electron micrographs of bare PLGA NPs (NP); pD-coated PLGA NPs (NP-pD); and QA-conjugated NP-pD (NP-pD-QA or QA-NP). Negative staining with 2% uranyl acetate. Scale bar: 100 nm.

prepared by the single emulsion solvent evaporation method. The bare NP was covered with a polymerized dopamine (pD) layer, which accommodated QA-NH_2 via Michael addition and/or Schiff base reactions,[27,28] to form QA-NP. The ESI-MS analysis of QA-NP (Figure S4, Supporting Information) provided qualitative evidence for successful conjugation of QA-NH_2 on QA-NP. PLGA NPs simply incubated with QA-NH_2 without pD functionalization (QA/NP) had no QA-NH_2 signature peaks on ESI-MS, confirming the essential role of pD coating as the mediator of QA-NH_2 conjugation. Transmission electron micrographs (TEM) (Figure 1b) identified a layer on the surface of the core NPs due to pD coating. However, there was no visible difference between NP-pD and NP-pD-QA (QA-NP) in the size and surface morphology, similar to previous examples using other ligands.[26] The number of QA-NH_2 conjugated to the surface of QA-NP was indirectly determined by subtracting the amount of QA-NH_2 remaining in the reaction medium from the original QA-NH_2 feed. The QA-NH_2 conjugated to unit surface area of QA-NP increased linearly with QA-NH_2 feed (Figure S5, Supporting Information) and did not saturate in the tested range. We attribute the efficient conjugation to hydrogen bonding between multiple hydroxyl groups of QA, which may allow for cooperative addition to the surface.

QA-NP had a *z*-average of 151 nm in diameter and a zeta potential of −11.8 mV according to dynamic light scattering (DLS) (**Table 1**, based on $n = 3$ independent batches). The particle size was larger than that estimated by TEM (100–120 nm) (Figure 1b). This difference is greater than the thickness of the typically attributed hydration layer, which is no more than a few nanometers, suggesting that the NPs underwent a mild degree of aggregation in the buffer in which the DLS measurement was performed. Prior to the biological evaluation of QA-NP, their size distribution in 50% fetal bovine serum (FBS) was tested at a NP concentration ranging from 0.05 to 0.2 mg mL^{-1}. Irrespective of the concentration, QA-NP showed a consistent peak at 120 nm (Figure S6a, Supporting Information), indicating the resolution of NP aggregation. The two distinctive peaks at 10 and 80 nm were identified to be serum proteins and their aggregates (Figure S6b, Supporting Information). Over 2 h in 50% FBS, no aggregation or agglomeration of QA-NP occurred. QA-NP could

Table 1. Particle size, zeta potential, and polydispersity index (PDI) of NPs. Data: mean ± s.d. ($n = 3$ independently and identically prepared batches).

Name	*Z*-average [*d*, nm]	Zeta potential [mV]	PDI
Bare NP	134 ± 12	−10.4 ± 9.3	0.1 ± 0.02
NP-pD	142 ± 17	−11.2 ± 8.1	0.2 ± 0.06
PEG-NP	163 ± 11	−10.7 ± 6.2	0.2 ± 0.04
PEG-NP (PLGA–DyLight 594)	167 ± 14	−12.1 ± 4.9	0.2 ± 0.07
QA-NP	151 ± 14	−11.8 ± 4.9	0.1 ± 0.03
QA-NP (PLGA–FITC)	149 ± 7	−9.3 ± 5.5	0.1 ± 0.03
QA-NP (PLGA–Alexa 555)	147 ± 11	−10.4 ± 6.1	0.1 ± 0.05
QA-NP (PLGA–ICG)	154 ± 20	−10.8 ± 5.7	0.1 ± 0.06
QA-NP (PLGA–DyLight 594)	158 ± 14	−11.6 ± 6.4	0.2 ± 0.03
Bare NP (PLGA–TPGS)	171 ± 33	−12.3 ± 6.6	0.2 ± 0.09
PTX@PEG-NP (PLGA–TPGS)	184 ± 41	−11.5 ± 5.7	0.2 ± 0.07
PTX@QA-NP (PLGA–TPGS)	179 ± 26	−10.8 ± 6.4	0.1 ± 0.04

be stored as lyophilized solid in 4 °C for up to one month without substantial changes in the physical properties (data not shown).

2.3. QA-NP Interact with Activated HUVECs

QA-NP interactions with endothelial cell layer were investigated with HUVECs. The HUVEC model was chosen on the basis of reported use as a cell model in the investigation of tumor–endothelial cell interactions.[29] QA-NP–HUVEC interaction was examined with confocal microscopy and flow cytometry (**Figure 2**a–c). Specifically, HUVECs were incubated with fluorescein (FITC)-labeled QA-NP or bare NP with or without tumor necrosis factor-alpha (TNF-α) treatment. A common condition for endothelial expression of selectins (10 ng mL^{-1} of TNF-α for 4 h) was followed.[30] Bare NPs were also tested in the same manner. Figure 2a shows that QA-NP were associated with the HUVECs with the majority on the cell membrane, whereas bare NPs showed minimal nonspecific binding. QA-NP were also observed in empty space between cells. Given that QA-NP did not bind to the plate without cells (Figure S7, Supporting Information), we speculate that soluble E-selectin secreted by the activated HUVECs[31] deposited on the plate surface and interacted with QA-NP. To quantify the NPs retained with the cells, fluorescence intensity of the cell suspension was measured by flow cytometry. Activated HUVECs incubated with QA-NP showed the greatest fluorescence intensity compared to control groups (nonactivated HUVECs with QA-NP (or bare NP) or activated HUVECs with bare NP), in agreement with confocal imaging. These results suggest that QA-NP have the affinity for the activated HUVECs and thus the potential to interact with the peritumoral endothelium.

To confirm the mediators of QA-NP and HUVEC interactions, the incubation was performed after pretreatment with free QA-NH_2, anti-E-selectin, or anti-P-selectin antibodies. QA-NP binding to the activated HUVECs was reduced by free QA-NH_2 (Figure 2d; Figure S8a, Supporting Information), anti-E-selectin (Figure 2e; Figure S8b, Supporting Information), and anti-P-selectin antibodies (Figure 2f; Figure S8c, Supporting Information) in a dose-dependent manner, which indicates that free QA-NH_2 competes with QA-NP and that the blockade of E-/P-selectin interferes with QA-NP binding to the activated HUVECs, respectively. These results confirm that the binding of QA-NP to the activated HUVECs was mediated by the QA interaction with E-/P-selectin.

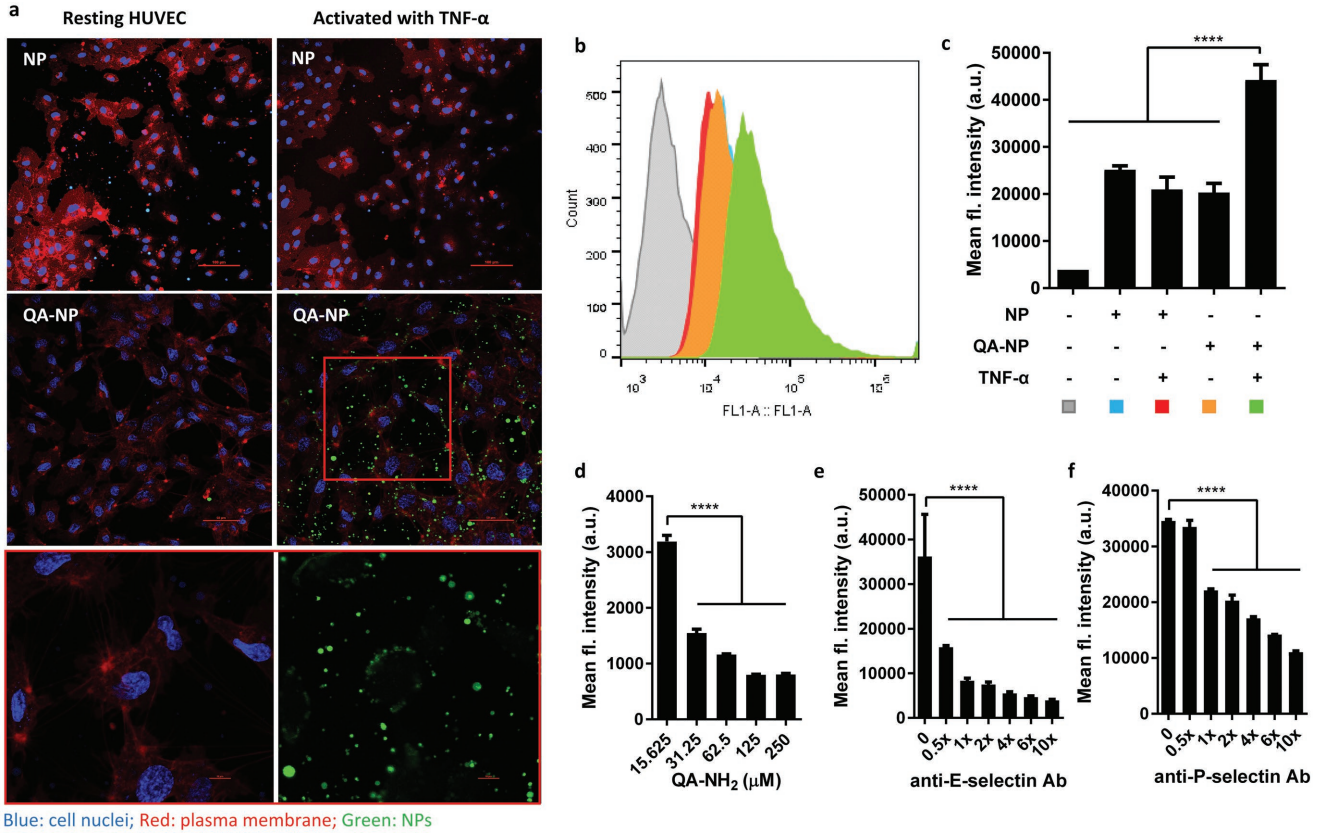

Figure 2. a) Confocal imaging of FITC-labeled NP and QA-NP incubated with resting or TNF-α-activated HUVECs. Green: NPs; blue: cell nuclei; red: plasma membrane. The box in QA-NP/activated HUVEC image was magnified at the bottom in two channels. b) Representative flow cytometry histogram. c) Quantitative measurement of HUVECs interacting with NP or QA-NP (n = 3 tests of a representative batch, mean ± s.d.). ****: $p < 0.0001$ versus QA-NP with TNF-α activated HUVEC by Dunnett's multiple comparisons test. Competitive inhibition of QA-NP binding to HUVECs by d) free QA-NH_2; e) anti-E-selectin antibody; and f) anti-P-selectin antibody. QA-NP to HUVEC binding was quantified by flow cytometry (n = 3 tests of a representative batch, mean ± s.d.). ****: $p < 0.0001$ by Dunnett's multiple comparisons test. The experiment was repeated with an independently and identically prepared batch of QA-NP, and the results are presented in Figure S8 (Supporting Information).

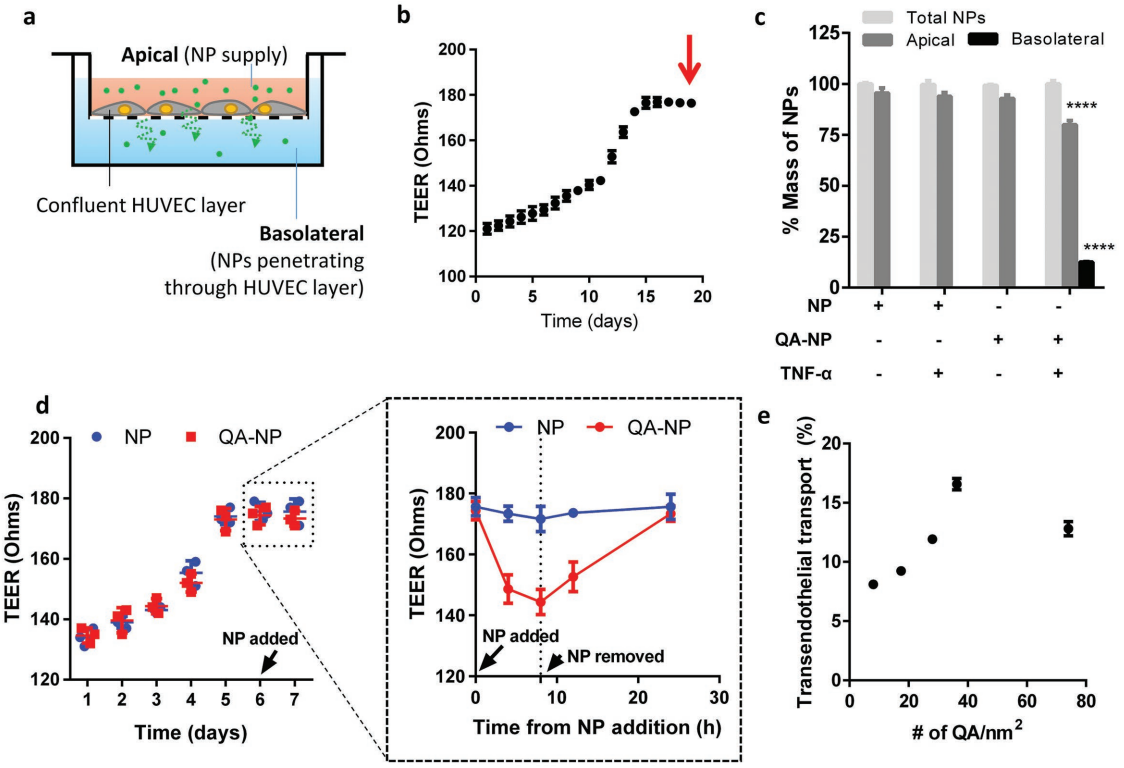

Figure 3. a) Schematic diagram of transendothelial transport of NPs. b) Representative TEER plot of HUVEC monolayer. The arrow indicates the time of NP addition. c) The percentage of NP transport across the confluent HUVEC monolayer with and without TNF-α activation (n = 3 test of a representative batch, mean ± s.d.). ****: $p < 0.0001$ versus NP with nonactivated HUVECs in each compartment by Holm–Sidak's multiple comparisons test. d) Representative TEER plot of HUVEC monolayer with values measured at shorter intervals from the time NP was added. The plot in a dashed box was magnified on the right. e) Relationship between the ligand density and the transendothelial transport of QA-NP (n = 3 tests of a representative batch, mean ± s.d.).

2.4. QA-NP Translocate Across the Activated HUVEC Layer Inducing Transient Increase in Endothelial Permeaiblity

We hypothesized that the interactions between QA-NP and the activated HUVEC would increase the chance for NPs to travel through the endothelial layer and reach the underlying tissues. To estimate this potential in vitro, we assessed the QA-NP transport across the endothelial cell layer grown on a Transwell insert (**Figure 3**a). We placed QA-NP and control NPs on the apical side of the Transwell containing a confluent HUVEC layer indicated by the transendothelial electrical resistance (TEER) values (Figure 3b), with and without TNF-α pretreatment, and quantified the NPs remaining in the apical side and those recovered from the basolateral side. As expected, the transport across the endothelial layer was observed only with QA-NP and TNF-α-activated (i.e., E-/P-selectin expressing) HUVECs (Figure 3c).

Literature suggests that the binding of antibodies or cancer cells to E-selectin enhances the transendothelial permeability and cell migration[32] by activating extracellular signal-regulated kinase and p38 mitogen-activated protein kinase, which initiate the disassembly of vascular endothelial–cadherin complexes.[33] We suspect that the binding of QA-NP to activated HUVECs may have enhanced transendothelial transport of QA-NP in a similar manner. To test if QA-NP treatment increased transendothelial permeability, we repeated the same experiment measuring TEER values after QA-NP or bare NP treatment with shorter intervals. With the addition of QA-NP (but not with bare NP), the TEER value immediately started to decrease over 8 h (Figure 3d). Once QA-NP was removed, the TEER value was gradually restored over the next 16 h. This result suggests that the transendothelial transport of QA-NP may be mediated by the transient increase in paracellular permeability of the endothelium due to the QA-NP binding to E-/P-selectins.

To examine the relationship between ligand density and the transendothelial transport, we measured the transport of QA-NP across the activated HUVECs varying the ligand densities (Figure 3e). QA-NP transport increased as the ligand density of QA-NP increased from 8 to 36 QA-NH_2 nm^{-2} but rather decreased with further increase of the ligand density to 74 QA-NH_2 nm^{-2}. We speculate that excess QA-NH_2 may have formed intermolecular clustering due to hydrogen bonding instead of interacting with selectins. Overall, the Transwell experiment supports that QA-NH_2 ligands with an optimal surface density help transport QA-NP across the activated HUVECs.

2.5. QA-NP Accumulate in Tumors with Forced Selectin Expression by Focal Irradiation

To test the distribution of QA-NP in vivo, we first used an animal model with forced E-/P-selectin expression via focal ionizing radiation.[12b,18,34] For comparison with traditional PEG-modified

NPs that depend mostly on the EPR effect, PEG-NP were prepared in the same manner as QA-NP except for the replacement of QA-NH_2 with PEG-NH_2 (Figure S9, Supporting Information). Balb/c mice were inoculated with syngeneic CT26 colon cancer cells on both hind limbs. One side was treated with 6 Gy of X-irradiation, and the other was left untreated. One day after intravenous (IV) injection of QA-NP or PEG-NP, tumors were collected and optically cleared for confocal imaging with the immunofluorescence staining of endothelial cells (anti-CD31), P-selectin, E-selectin, and macrophages (anti-F4/80).[35] QA-NP displayed greater accumulation in tumor than PEG-NP, even in the absence of irradiation (**Figure 4**; Figure S10, Supporting Information). The difference apparently increased in the irradiated tumors, which manifested stronger E- and P-selectin stains, indicating that QA-NP accumulation in tumor increased with selectin expression. The irradiated tumors also showed an increased population of macrophages (a response to irradiation-induced inflammation[36]); however, we exclude the possibility of the tumor-associated macrophages mediating NP uptake[37] for the following reasons: i) PEG-NP accumulation remained negligible in the irradiated tumor despite the increased macrophage population (Figure 4; Figure S10a, Supporting Information), ii) there is little overlap between QA-NP and F4/80$^+$ cells (Figure S10b, Supporting Information), and iii) our in vitro study suggested that the surface QA suppresses the macrophage uptake of QA-NP (Figure S11, Supporting Information), likely due to the multiple hydroxyl groups increasing the hydrophilicity of the surface. It is worth noting that, at the time of observation, both E- and P-selectin signals were not colocalized with CD31 but rather seen with macrophages. This may reflect

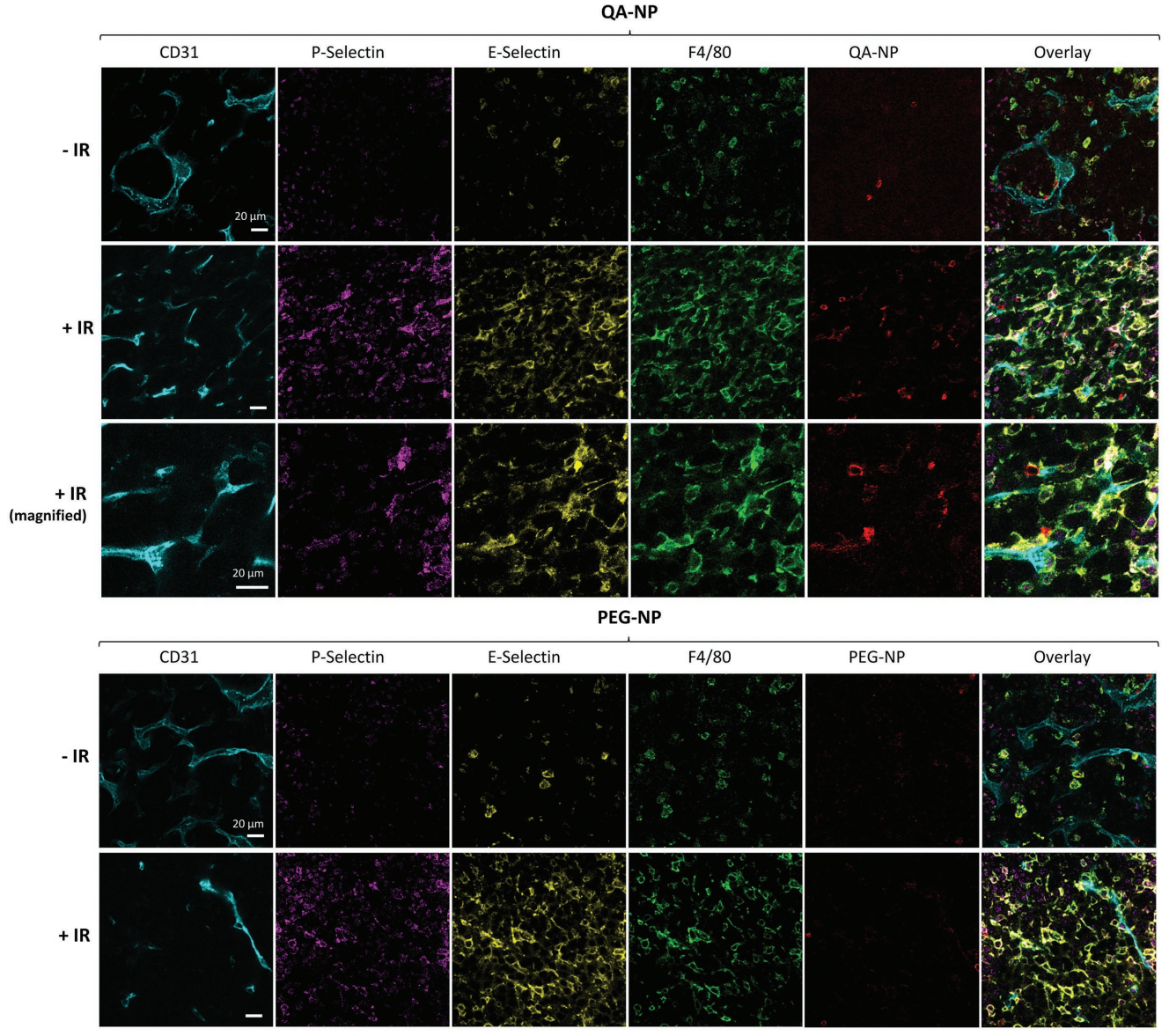

Figure 4. Confocal imaging of optically cleared, antibody-stained CT26 tumor sections from animals receiving QA-NP (top) and PEG-NP (bottom), with or without 6 Gy X-irradiation (± ionizing radiation, ± IR). Tumors were sampled one day after injection. Different views of each section are shown in Figure S10 (Supporting Information). $n = 2$ mice per NP, 2 sections per mouse.

the transient nature of selectin expression on endothelial surface[38,39] and the macrophage uptake of the secreted selectins. To observe QA-NP transport in cancer models with more stable expression of endothelial selectins, we next screened cancer cells that may induce selectin expression in the endothelial cells.

2.6. Cancer Cells Induce Endothelial Selectin Expression

Endothelial expression of selectins is induced by cytokines from the neighboring cells.[15a,40] To examine whether cancer cell lines have such paracrine effects on endothelial cells, we incubated endothelial cells in the media conditioned with various cancer cells of matching species and measured the E-/P-selectin expression. All the tested human cell lines induced the expression of selectins in HUVECs (Figure S12a,b, Supporting Information). MDA-MB-231-conditioned medium induced E-selectin expression to the greatest extent, followed by MCF-7-conditioned medium. P-selectin expression was the greatest with MCF-7-conditioned medium, then with MDA-MB-231 and A2780-conditioned media. Similarly, murine B16F10 and 4T1 cells induced significant expression of E-/P-selectin in mouse hemangioendothelioma (EOMA) cells (Figure S12c,d, Supporting Information). These results support broad applicability of E-/P-selectin targeting. As the MDA-MB-231-conditioned medium induced both E- and P-selectin expressions, we chose a mouse model of MDA-MB-231 xenograft for subsequent in vivo evaluation of QA-NP. Among murine cell lines, B16F10 cells were used to make a syngeneic model of melanoma for additional evaluation of PTX@QA-NP. E-/P-selectin expression in MDA-MB-231 tumor was confirmed by immunohistochemistry (Figure S13, Supporting Information) as well as intravital imaging in live animals (Figure S14, Supporting Information). In the intravital imaging, E-/P-selectin expression was mainly observed in the blood vessel unlike immunohistochemistry of MDA-MB-231 model or clinical samples,[14] which showed broader selectin distribution. This difference may be explained by the way the selectins were stained. While immunohistochemistry stains the sectioned tissues letting the tumor tissues contact antibodies, intravital imaging provides antibodies through circulation, where the antibodies are likely to bind first to the endothelium without proceeding further.

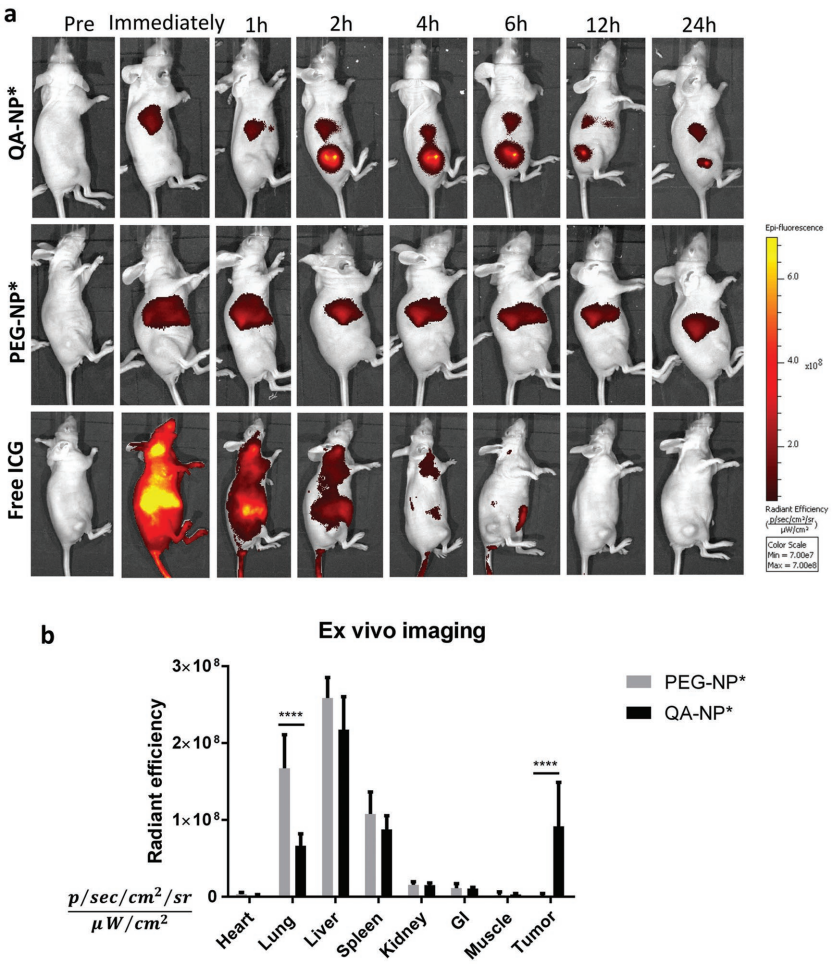

Figure 5. a) Representative whole body imaging of animals over 24 h from the injection of each treatment. Animals bearing subcutaneous MDA-MB-231 tumor xenografts were treated with QA-NP* (top), PEG-NP* (middle), and free ICG (bottom) by tail vein injection. See Figure S16 (Supporting Information) for all animals receiving the treatments. b) Fluorescence intensity of ex vivo images of major organs retrieved at the end of whole body imaging (24 h postinjection). $n = 5$ mice per group. ****: $p < 0.0001$ by Bonferroni's multiple comparisons test following two-way ANOVA.

2.7. In Vivo Fluorescence Imaging Shows QA-NP Distribution

On the basis of the above in vitro results, we hypothesized that QA-NP might develop active interactions with peritumoral endothelium via E-/P-selectin, translocate across the activated endothelium, as it did with the activated HUVEC, and accumulate in MDA-MB-231 tumors to a greater extent than PEG-NP. To trace the NP distribution over time by whole body fluorescence imaging, we labeled QA-NP with indocyanine green (ICG), a near infrared fluorescence dye, by conjugating the dye to PLGA via carbodiimide chemistry. NPs made with the PLGA–ICG conjugate (ICG-NP) remained stable in 50% FBS in contrast to those physically encapsulating ICG (ICG/NP) (Figure S15, Supporting Information), indicating that the fluorescence of the ICG-NPs would represent NPs in the whole body imaging.

The ICG-labeled (indicated as *) QA-NP and PEG-NP or free ICG with equivalent fluorescence intensity were injected via tail vein and imaged over 24 h (**Figure 5**a; Figure S16, Supporting Information). Free ICG spread throughout the body immediately following the administration and gradually disappeared by hepatobiliary elimination.[41] On the other hand, QA-NP* and

PEG-NP* showed up in the liver immediately after the injection. Significant tumor accumulation of QA-NP* was observed starting at 2 h postinjection, whereas nearly no fluorescence was detected in animals treated with PEG-NP*, let alone free ICG. The QA-NP* signal in the tumor gradually decreased over time but persisted throughout the 24 h experiment period (Figure S17, Supporting Information). Animals receiving PEG-NP* and free ICG did not show fluorescence in tumors at all time points. It is curious that PEG-NP* was not observed at all in the tumor. Although not as vascularized as highly angiogenic LS174T xenografts[42] (Figure S18, Supporting Information), MDA-MB-231 xenograft is still more vascularized than muscle tissues, according to the extent of Evans blue accumulation (LS174T/muscle = 1.34, MDA-MB-231/muscle = 1.04), in accordance with the literature.[43] We speculate that the fluorescence detection threshold was set too high to capture weak fluorescence intensity of tumors with PEG-NP*. Major organs were excised and imaged ex vivo 24 h postinjection. Consistent with live whole body imaging, animals receiving PEG-NP* showed the greatest fluorescence signal in the liver, followed by the lung and spleen (Figure 5b). QA-NP* showed less accumulation in the reticuloendothelial system (RES) and significantly higher tumor signals than PEG-NP*. This result was confirmed in another set of animals (Figure S19, Supporting Information). The ex vivo imaging obtained at 6 h postinjection showed a similar trend as 24 h postinjection, except for the relative distribution of PEG-NP* in the RES organs. Although the contribution of the EPR effect may not be excluded, the superior tumor accumulation of QA-NP* relative to PEG-NP*, consistently shown in Figures 4 and 5, indicates that the selectin-mediated transport plays a dominant role in tumor distribution of QA-NP.

To investigate whether the interaction between QA-NP and E-/P-selectin helped QA-NP to extravasate and enter tumors, we used intravital microscopy to visualize QA-NP in mice with GFP-expressing MDA-MB-231 tumors. QA-NP was observed from 2 h postinjection near the blood vessel, and the signal increased over time indicating gradual accumulation of QA-NP in the tumor (**Figure 6**). This observation agrees with in vitro Transwell result and provides an in vivo proof-of-concept that QA-NP interaction with E-/P-selectin improved extravasation and enhanced tumor accumulation. It is worth noting that most QA-NP were nevertheless observed near the vasculature, which indicates limited intratumoral transport of the NPs. Given that efficient tumor penetration was reported with NPs of 50 nm or smaller,[44] further reduction of NP size may be necessary to improve intratumoral transport of QA-NP. Alternatively, conditionally disintegrated assemblies of ultrasmall NPs[45] are also conceivable to afford both long-term circulation (favoring relatively large size[44c]) and deep intratumoral penetration (favoring small size[44c]).

2.8. PTX-Loaded QA-NP Demonstrates Greater In Vivo Anticancer Efficacy than Taxol or PEGylated NPs

2.8.1. Production of PTX-Loaded QA-NP

We next examined whether QA-NP would deliver PTX, a model anticancer drug, better than PEG-NP and achieve superior anticancer efficacy. Typical PTX loading efficiency in PLGA NPs is no more than 5 wt%.[46] The low drug loading increases the NP dose requirement and thus the concentration and/or volume of injection, posing technical challenges in administration. To increase the drug loading capacity, we used a conjugate of PLGA and tocopheryl polyethylene glycol 1000 succinate (PLGA–TPGS) instead of PLGA following the reported method.[47] PLGA–TPGS was synthesized by ring opening polymerization and confirmed by ^{1}H NMR (Figure S20, Supporting Information) and matrix-assisted laser desorption/ionization-MS (MALDI-MS). The molecular weight (MW) ranged 4–8 kDa with an average of 5 kDa according to MALDI-MS (Figure S21, Supporting Information). NP made of PLGA–TPGS showed greater PTX loading (13.0 ± 0.2%) than those made of $PLGA_{150k}$ (loading efficiency: 4.0 ± 0.01%) or $PLGA_{30k}$ and physically stabilized by TPGS ($PLGA_{30k}$/TPGS, loading efficiency: 9.6 ± 0.5%) (Figure S22a, Supporting Information). Release kinetics performed in phosphate-buffered saline (PBS) containing 0.2% Tween 80 showed that in 48 h PTX@NP (PLGA–TPGS) released 59.8 ± 3.5% of the loaded PTX; PTX@NP ($PLGA_{30k}$/TPGS) 79.1 ± 9.8%; and PTX@NP ($PLGA_{150k}$) 46.8 ± 0.5% (Figure S22b,c, Supporting Information). TEM images showed

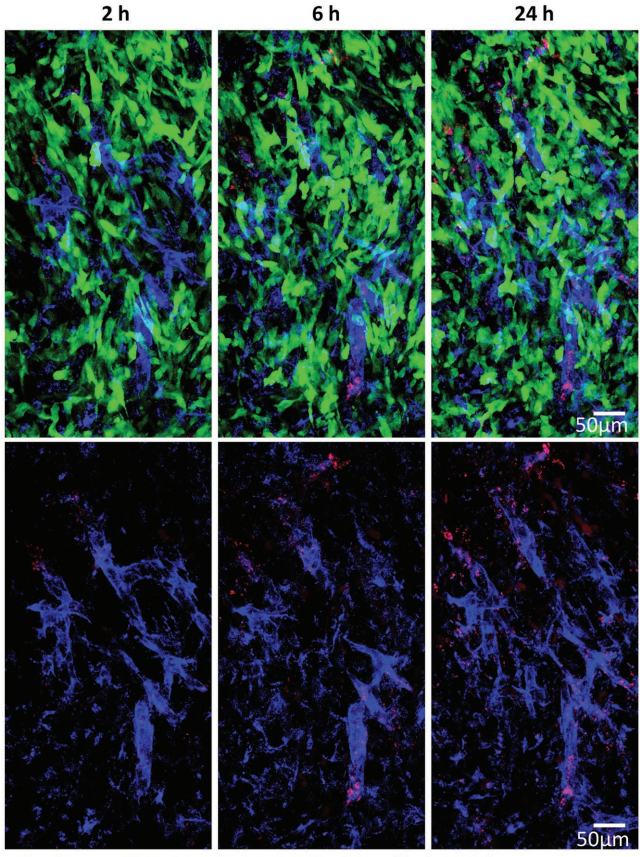

Figure 6. Intravital microscopy images of GFP-expressing MDA-MB-231 tumor in a dorsal skinfold chamber after 2, 6, and 24 h after IV injection of Alexa Fluor 555-labeled QA-NP. Top: Overlays of blood vessels (blue), QA-NP* (red), and MDA-MB-231-GFP tumor cells (green). Bottom: Overlays of blood vessels and QA-NP only.

no significant morphological difference between NPs made of PLGA and those of PLGA–TPGS (Figure 1 vs Figure S23, Supporting Information). To confirm the functionality of QA-conjugated PLGA–TPGS NPs, QA-NPs made of regular PLGA or PLGA–TPGS (and bare NPs made of respective polymers as negative controls) were used as competitive inhibitors for the binding of FITC-labeled QA-NP to the activated HUVECs. The binding was not affected by the added bare NPs but decreased with the addition of QA-NPs in a dose-dependent manner, irrespective of the polymer type used for the core NPs (Figure S24, Supporting Information). This result indicates that core NPs did not affect the surface functionality and PLGA–TPGS NPs might serve as a valid substitute for PLGA NPs as core particles. It also demonstrates the robustness and broad applicability of QA conjugation process and suggests the potential for modular design of QA-modified NPs. On the basis of high drug loading and consistent surface functionality, we used PLGA–TPGS in producing PTX-loaded QA-NP (PTX@QA-NP) for the subsequent in vivo studies. Free PTX, a physical mixture of PTX and blank QA-NP, and PTX@QA-NP showed similar half maximal inhibitory concentration (IC_{50}) values in MDA-MB-231 cells, confirming that QA-NP itself had no additional toxicity (Figure S25, Supporting Information).

2.8.2. Design of Anticancer Efficacy Studies

The anticancer efficacy of PTX@QA-NP was tested in comparison with Taxol, a commercial surfactant-solubilized PTX formulation, and PTX@PEG-NP, a control NP without QA modification. The maximum tolerated dose of PTX@QA-NP was first determined. Healthy female nude mice survived 10 injections of PTX@QA-NP at PTX 30 mg kg^{-1} per dose over 2 weeks without a significant weight loss (Figure S26, Supporting Information). Since the reported maximum tolerated dose of Taxol was relatively low (20 mg kg^{-1} PTX equivalent, qd × 5),[48] the evaluation of QA-NP in vivo anticancer efficacy was performed in two different settings: one compared with Taxol at its known tolerated doses (20 mg kg^{-1} PTX equivalent, single administration or q3d × 5 at 20 mg PTX kg^{-1} per dose over 2 weeks) and the other compared with PTX@PEG-NP at the NP's maximum tolerated dose (30 mg kg^{-1} per dose × 10 times over 2 weeks).

2.8.3. Anticancer Efficacy: PTX@QA-NP versus Taxol

The anticancer efficacy of PTX@QA-NP was first tested with a single dose (20 mg kg^{-1} PTX equivalent) in a female nude mouse model of subcutaneous MDA-MB-231 tumor. Taxol was used at the same dose as a reference. As shown in **Figure 7**a, PTX@QA-NP attenuated the growth of MDA-MB-231 tumors more efficiently than Taxol. The median survival time of animals receiving PTX@QA-NP was 62 days, significantly longer than that of Taxol (44 days, $p < 0.01$, Log-rank test). The same regimen was administered to male C57BL/6 mice with syngeneic B16F10 tumors (Figure S27, Supporting Information). Reflecting the known aggressive nature,[49] the B16F10 tumors grew much faster than MDA-MB-231 tumors, but PTX@QA-NP still induced superior tumor attenuation to Taxol at the same dose.

Next, PTX@QA-NP was given every three days over 2 weeks (total five times: q3d × 5) at 20 mg kg^{-1} per dose (Figure 7b). PTX@QA-NP offered a significant survival benefit with complete remission in 60% (3 out of 5) animals by 357 days (as of the submission of this report), while only one surviving in the Taxol group during the same period. Two animals treated with Taxol reached the end point based on the tumor size, one with deteriorating health condition with an ulcerated tumor, and the other found dead with no apparent reason. These results collectively demonstrate that PTX@QA-NP brings greater anticancer efficacy than Taxol at the equivalent dose.

2.8.4. Anticancer Efficacy: PTX@QA-NP versus PTX@PEG-NP

PTX@QA-NP was compared with PTX@PEG-NP (both made with PTX@PLGA–TPGS core particles) at the maximum tolerated dose. Female nude mice with subcutaneous MDA-MB-231 animals were treated with 10 injections of one of the following treatments over the period of 2 weeks: i) saline; ii) blank QA-NP; iii) blank PEG-NP; iv) PTX@PEG-NP at 30 mg PTX kg^{-1} per dose; and v) PTX@QA-NP at 30 mg PTX kg^{-1} per dose. Only the PTX@QA-NP group showed a survival benefit compared to the saline group, with 40% complete remission as of 367 days (as of the submission of this report) (**Figure 8**a). All other groups succumbed to death with a median survival time of 68 days (saline), 86 days (blank QA-NP), 80 days (blank PEG-NP), and 70 days (PTX@PEG-NP). It was surprising that the PTX@PEG-NP group was no better than the negative control groups and had no surviving animals. We reasoned that PTX@PEG-NP might have induced the production of anti-PEG antibodies. The accelerated blood clearance (ABC) phenomemon due to anti-PEG IgM is well documented with PEGylated liposomes and shown to be responsible for rapid elimination of repeatedly administered liposomes.[50] The extent of ABC may vary with the extent of modification, and the length and density of PEG, but since it has been reported with different types of NP systems,[51] we infer that anti-PEG antibodies may have accelerated the clearance of subsequently dosed PTX@PEG-NPs. To investigate this possibility, we treated healthy nude mice with saline, blank PEG-NP, or blank QA-NP, collected blood 5 days later, and added the serum to a plate coated with mPEG or QA to determine the presence of antibodies. Animals receiving PEG-NP produced antibodies that bound to PEG-decorated surface, while other treatments (saline, QA-NPs) did not (Figure 8b). QA-NP injection did not induce the production of anti-QA antibodies. These results demonstrate that QA-NP delivered PTX to tumors more efficiently than PEG-NP by repeated administration.

2.8.5. Pharmacokinetics and Biodistribution of PTX Delivered by QA-NP and PEG-NP

Pharmacokinetics (PK) and biodistribution of PTX were compared following a single IV injection of PTX@QA-NP and PTX@PEG-NP at a dose equivalent to PTX 20 mg kg^{-1}. The two NPs

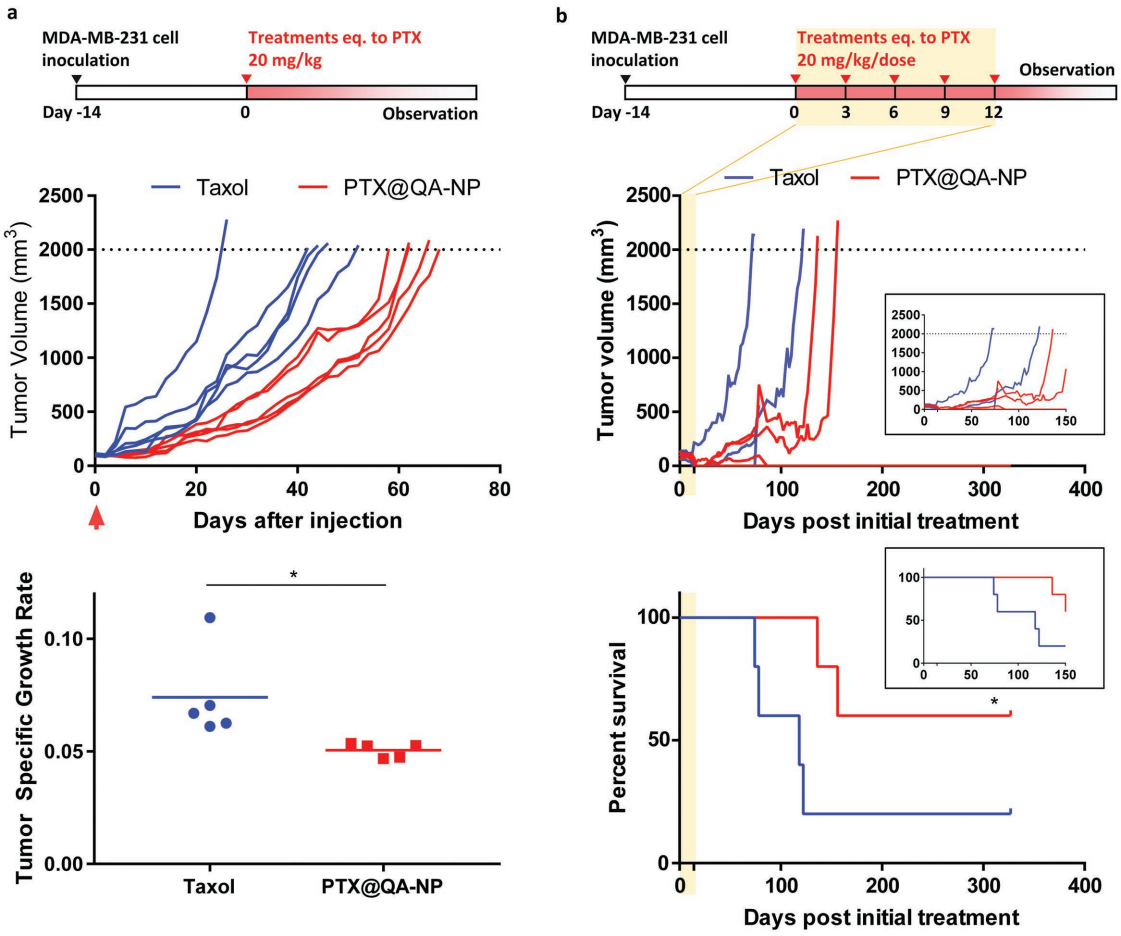

Figure 7. Anticancer efficacy of PTX@QA-NP and Taxol in female nude mice with MDA-MB-231 xenografts. a) Treatments given as a single dose equivalent to PTX 20 mg kg^{-1}. Mice were sacrificed once the tumor volume (V) reached 2000 mm^3 or showed any signs of morbidity defined in the animal protocol. $n = 5$ mice per group. Tumor specific growth rate is defined as $\Delta \log V/\Delta t$ (t: time in days). *: $p < 0.05$ by unpaired t-test. b) Treatments given as five doses of 20 mg PTX equivalent per kg per dose over 2 weeks. $n = 5$ mice per group. *: $p < 0.05$ by Gehan–Breslow–Wilcoxon test. Inset graphs show the tumor growth and survival over 150 days.

showed similar PK profiles and comparable plasma PK parameters upon noncompartmental analyses (**Table 2** and Figure 8c). However, PTX@QA-NP resulted in a significantly higher PTX concentration in tumor than PTX@PEG-NP (7119 ng g^{-1} for PTX@QA-NP and 145.5 ng g^{-1} for PTX@PEG-NP), when measured at 24 h after IV injection, whereas PTX concentration in other major organs remained comparable (Figure 8d). This result is consistent with the superior anticancer efficacy of PTX@QA-NP relative to PTX@PEG-NP (Figure 8a). The PTX distribution did not exactly mirror the ex vivo imaging, which showed the semiquantitative NP distribution at 24 h postinjection (Figure 5b). This discrepancy may be explained by the preferential removal of PTX from the RES organs, such as hepatic metabolism[52] and/or PTX redistribution following phagocytic degradation.

3. Conclusion

QA was conjugated on the surface of PLGA NPs to promote the extravasation of the NPs via the interaction with selectin-expressing peritumoral endothelium. The QA-decorated NPs (QA-NP) interacted with selectin-expressing HUVECs and translocated across the confluent HUVEC layer. QA-NP showed greater accumulation and PTX delivery in selectin-expressing tumors as compared to PEG-NP. PTX-loaded QA-NP showed greater anticancer efficacy than Taxol or PTX-loaded PEG-NP at equivalent PTX doses, leading to complete tumor remission in 40–60% of MDA-MB-231 tumor-bearing mice by repeated dosing over 2 weeks. The superior anticancer efficacy of QA-NP is also partly due to the lack of antibody formation. Our results support that QA-NP can exploit the interaction with selectin-expressing peritumoral endothelium and deliver anticancer drugs to tumors to a greater extent than conventional PEG-NP.

4. Experimental Section

Materials: PLGA (LA:GA = 85:15, acid endcap, MW: 150 kDa), PLGA (LA:GA = 50:50, acid endcap, MW: 30 kDa), FITC-conjugated PLGA (LA:GA = 48:52, MW: 5 kDa), and PLGA-ethylenediamine (PLGA-NH_2, LA:GA = 57:43, MW: 5 kDa) were purchased from Akina, Inc. (West Lafayette, IN, USA). Indocyanine green-N-succinimidyl ester (ICG-NHS) was purchased from Intrace medical (Lausanne, Switzerland). Hoechst

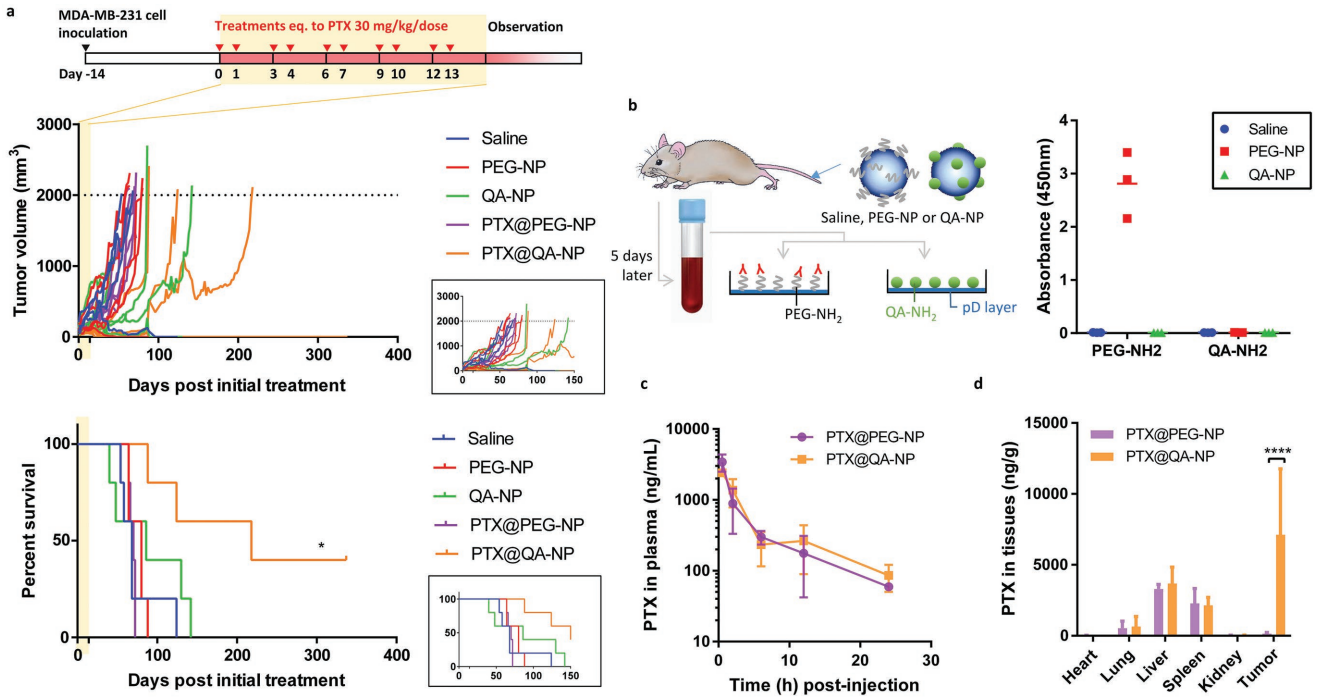

Figure 8. a) Anticancer efficacy of PTX@QA-NP, compared with those of saline, blank PEG-NP, blank QA-NP, and PTX@PEG-NP. Treatments were given as 10 doses of 30 mg PTX equivalent per kg per dose over 2 weeks. $n = 5$ mice per treatment. *: $p < 0.05$ by Log-rank (Mantel-Cox) test. Inset graphs show the tumor growth and survival over 150 days. b) Formation of antibodies to each ligand (PEG, QA), detected at 5 days after a single injection of PEG-NP, QA-NP, or saline (as a negative control). $n = 3$ mice per group. c) Plasma PTX concentration profile after a single injection of PTX@QA-NP or PTX@PEG-NP at a dose equivalent to 20 mg kg^{-1} PTX in MDA-MB-231 xenograft-bearing mice. $n = 3$ mice per time per group. d) Biodistribution of PTX in major organs 24 h after a single injection of PTX@QA-NP or PTX@PEG-NP at a dose equivalent to 20 mg kg^{-1} PTX in MDA-MB-231 xenograft-bearing mice. $n = 3$ mice per group. ****: $p < 0.0001$ by Sidak's multiple comparisons test.

33342 and recombinant human TNF-α were purchased from Invitrogen (Eugene, OR, USA). Methoxy-polyethylene glycol-amine (mPEG-NH_2, MW: 5 kDa) was purchased from JenKem Technology USA (Allen, TX, USA). Collagen I rat-tail, Vacutainer PST Tubes with spray-coated lithium heparin and a gel for plasma separation, Vacutainer Plus Plastic Serum Tubes with spray-coated silica for serum separation, and Calcein AM were purchased from BD Biosciences (San Jose, CA, USA). Dopamine hydrochloride was purchased from Alfa Aesar (Ward Hill, MA, USA). CellMask deep red membrane staining dye, Alexa Fluor 555 NHS ester (succinimidyl ester), DyLight 594-NHS ester, goat anti-mouse IgM secondary antibody, HRP-conjugated, Gibco Dulbecco's modified eagle's medium (DMEM), Gibco Eagle's minimum essential complete medium (EMEM), Gibco RPMI 1640 medium (RPMI), and Gibco Iscove's modified Dulbecco's medium were purchased from ThermoFisher Scientific (Waltham, MA, USA). Endothelial cell growth medium EGM-2 BulletKit was purchased from Lonza, Inc. (Williamsport, PA, USA). E-selectin antibody (P2H3) FITC, E-selectin antibody (UZ5) FITC, P-selectin antibody (CTB201), and P-selectin antibody (CTB201) FITC were purchased from Santa Cruz (Dallas, TX, USA). Transwell polycarbonate membrane cell culture inserts (6.5 mm) with 3.0 µm pore were purchased from Corning (Corning, NY, USA). PTX was a generous gift from Samyang Biopharm (Seongnam, South Korea). All other materials were purchased from Sigma-Aldrich (St. Louis, MO, USA).

Table 2. Plasma PK parameters of PTX@PEG-NP and PTX@QA-NP. PK parameters were obtained from noncompartmental analyses. The numbers in parentheses denote the standard errors (SE) associated with estimated parameters.

PK parameter	Formulation	
	PTX@PEG-NP	PTX@QA-NP
$t_{1/2}$ [h]	7.7	5.4
C_{max} [µg mL^{-1}]	3.4 (0.5)	2.4 (0.05)
$AUC_{0\text{-last}}$ [h µg mL^{-1}]	10.6 (0.4)	11.0 (0.1)
$AUC_{0\text{-}\infty}$ [h µg mL^{-1}]	11.3	11.6
MRT [h]	5.8	6.3
CL [L h^{-1} kg^{-1}]	1.8	1.7
V_{ss} [L kg^{-1}]	10.4	11.0

Synthesis of QA-NH_2 (Scheme S1, Supporting Information)—(1S,3R,4S,5R)-1,3,4,5-tetraacetoxycyclohexane-1-carboxylic acid (Compound 2): Quinic acid (compound 1, 961 mg, 5 mmol) was dissolved in 12 mL of acetic anhydride–pyridine 1:2 mixture. The solution was mixed with 4-dimethylaminopyridine (20 mg, 0.16 mmol) and stirred for 12 h at 5 °C. The reaction mixture was then added to ice water, acidified to pH 3 and extracted with dichloromethane (DCM). The extract was dried with sodium sulfate and concentrated to give a white solid (1.75 g, 97% Yield). ESI: $(M+H)^+$: 361.

(1R,2S,3R,5S)-5-((3-amino-5-(methoxycarbonyl)phenyl)carbamoyl) cyclohexane-1,2,3,5-tetrayl tetraacetate (Compound 3): Compound 2 (958 mg, 2.7 mmol) was dissolved in 15 mL of dimethylformamide (DMF). The solution was mixed with N-hydroxybenzotrizole (432 mg, 3.2 mmol) and stirred for 5 min at 0 °C. (1-ethyl-3-[3-dimethylaminopropyl] carbodiimide (612 mg, 3.2 mmol) and triethyl amine (0.5 mL, 4.3 mmol) were then added to the mixture and stirred for 1 h at 0 °C. Finally, a solution of methyl 3,5-diaminobenzoate (1.7 g, 7.7 mmol) in DMF (5 mL) was added to the mixture, which was warmed up to room temperature and stirred for 72 h. The reaction mixture was then added to ice water and extracted with DCM. The extract was dehydrated with sodium sulfate,

filtered, and further evaporated. The residue was purified by column chromatography on silica gel (hexane-ethyl acetate 3:7) to yield a brown solid compound (1.3 g, 92% Yield). ESI: $(M+H)^+$: 509.

3-Amino-5-((1S,3R,4S,5R)-1,3,4,5-tetrahydroxycyclohexane-1-carboxamido)benzoic acid (Compound 4): A solution of compound 3 (102 mg, 0.2 mmol) in tetrahydrofuran (5 mL) was stirred with lithium hydroxide monohydrate (63 mg, 1.5 mmol) for 48 h at room temperature. The reaction mixture was then acidified to pH 5 using Amberlite acidic resin, filtered, and purified by reverse column chromatography on C_{18}-reversed phase silica gel (water–acetonitrile (ACN) 1:2) to yield a white solid compound (45 mg, 69% Yield). ESI: $(M+H)^+$: 327.

Synthesis of ICG-Conjugated PLGA, Alexa Fluor 555-Conjugated PLGA, and DyLight 594-Conjugated PLGA: 200 mg of PLGA-ethylene diamine were dissolved in 2 mL dimethyl sulfoxide (DMSO) at room temperature. 1.5 mg of ICG-NHS, Alexa Fluor 555-NHS, or DyLight 594-NHS was dissolved in 1 mL DMSO at room temperature with rigorous vortex mixing. 1 mL of N,N-diisopropylethylamine was added to PLGA solution, followed by dropwise addition of ICG-NHS, Alexa Fluor 555-NHS or DyLight 594-NHS solution. The mixture was constantly stirred for 2 h, put in a regenerated cellulose dialysis bag with a MW cut off 3500 Da (Spectrum Labs, Rancho Dominguez, CA, USA) and dialyzed against excess DMSO 3 times and DCM 3 times. The purified sample was collected via rotary evaporation and stored at –20 °C.

Synthesis of TPGS-Conjugated PLGA (PLGA–TPGS): Glycolide 1 g, lactide 1 g, D-α-tocopherol polyethylene glycol 1000 succinate (TPGS) 400 mg were dissolved in toluene containing 0.5 wt% stannous octoate. The reaction was carried out at 145 °C under oxygen- and moisture-free environment for 16 h. The resulting product was dissolved in DCM and then precipitated in excess cold methanol to separate unreacted reagents. The final product, PLGA–TPGS, was collected by filtration, washed twice with distilled water, and dried under vacuum at 60 °C for 72 h.

Preparation of Bare NP: Bare NP was produced by the single emulsion solvent evaporation method. In brief, 100 mg of PLGA was dissolved in 4 mL of DCM. The polymer solution was added to 12 mL of a 5% polyvinyl alcohol (PVA) solution and emulsified using a Sonics Vibracell probe sonicator (Sonics, Newtown, CT, USA) for 2 min. The emulsion was added to 40 mL of deionized (DI) water and stirred for 4 h to evaporate DCM. The NP was then collected by an Optima MAX-XP ultracentrifuge (Beckman Coulter, Brea, CA, USA) at 34 000× g and washed with DI water three times. For confocal microscopy and flow cytometry, NP was prepared with FITC-conjugated PLGA. For imaging of NPs in focally irradiated tumors, NP was prepared with DyLight 594-conjugated PLGA.

For optical in vivo imaging, NP was prepared with ICG-conjugated PLGA. For intravital microscopy, NP was made with Alexa Fluor 555-conjugated PLGA. PTX-encapsulated NPs (PTX@NP) were prepared with $PLGA_{150k}$, $PLGA_{30k}$, and PLGA–$TPGS_{5k}$. For PTX@NP with $PLGA_{150k}$ (PTX@NP ($PLGA_{150k}$)), 20 mg of $PLGA_{150k}$ and 2 mg of PTX were dissolved in 1 mL of DCM, homogenized in 4 mL of 5% PVA by probe sonication (2 min, with 4 s on, 2 s off at 40% amplitude), and stirred in 20 mL of DI water overnight. For PTX@NP with $PLGA_{30k}$, 20 mg of $PLGA_{30k}$ and 2 mg of PTX dissolved in 1 mL of DCM were homogenized in 4 mL aqueous solution containing 0.5% PVA and 0.1% TPGS, and stirred in 20 mL of 0.5% PVA overnight. To indicate the use of TPGS as an emulsifier, we called the NPs PTX@NP ($PLGA_{30k}$/TPGS). PTX@NP with PLGA–$TPGS_{5k}$ (PTX@NP (PLGA–$TPGS_{5k}$)) was prepared by homogenizing 1 mL DCM solution of 20 mg of PLGA–$TPGS_{5k}$ and 2 mg of PTX in 4 mL of 5% PVA and stirring in 20 mL of DI water. The NPs were collected via ultracentrifugation, and washed three times prior to freeze drying.

NP Surface Modification: The core NPs were coated with pD by 3 h incubation in 2 mL of dopamine hydrochloride solution in Tris buffer (10×10^{-3} M, pH 8.5) at room temperature with rotation. The pD-coated PLGA NPs (NP-pD) were collected by ultracentrifugation and washed twice with DI water. For further surface functionalization, NP-pD were resuspended in Tris buffer containing QA-NH_2 or mPEG-NH_2, maintaining the weight ratio of NP-pD to the ligands at 1:2 unless specified otherwise. After 30 min incubation, the NPs were collected via ultracentrifugation and washed with DI water twice. The surface-functionalized NPs were designated as QA-NP (or NP-pD-QA) and PEG-NP (or NP-pD-PEG), respectively.

Physical Characterization of NPs: NPs were dispersed in phosphate buffer (1×10^{-3} M, pH 7.4), and their sizes and zeta potentials were measured by a Malvern Zetasizer Nano ZS90 (Worcestershire, UK). NP morphology was observed by Tecnai transmission electron microscopy (FEI, Hillsboro, OR, USA) after negative staining with 2% uranyl acetate. QA-NH_2 surface decoration was confirmed by ESI-MS analysis of QA-NP. PEG-NH_2 surface decoration was confirmed by MALDI-TOF MS.

QA-NH_2 Ligand Density on NPs: A known amount of NP-pD was resuspended in Tris buffer (10×10^{-3} M, pH 8.5) containing a known amount of QA-NH_2 (QA-NH_2 feed). After 30 min incubation, the NP was collected via ultracentrifugation, and the supernatant was analyzed by an Agilent 1100 high-pressure liquid chromatography (HPLC) system (Palo Alto, CA, USA) equipped with Ascentis C18 column (25 cm × 4.6 mm, particle size: 5 µm) to quantify unconjugated free QA-NH_2. The mobile phase was a 90:10 volume mixture of water and ACN and eluted at 0.5 mL min^{-1}. QA-NH_2 was detected by a UV detector at the wavelength of 227 nm. The surface-conjugated QA-NH_2 was calculated by subtracting the unconjugated QA-NH_2 from the QA-NH_2 feed. The QA-NH_2 ligand density (QA-NH_2 per nm^2) was calculated as the number of surface-conjugated QA-NH_2 divided by the total surface area of NP-pD.

NP Stability in Serum: For evaluation of size stability, 5 mg of QA-NP were suspended in 5 mL of 50% FBS and incubated for 2 h at room temperature. Particle size distribution was measured by a Malvern Zetasizer Nano ZS90. For evaluation of fluorescence stability, ICG-labeled QA-NP was suspended in 50% FBS. NP pellet and supernatant were separated by ultracentrifugation at prespecified time points and imaged with IVIS Lumina to detect fluorescence intensity.

PTX Loading Efficiency: NPs with a premeasured mass were dissolved in 50% ACN at a concentration of 50 µg mL^{-1} and filtered with 0.45 µm polyvinylidene fluoride (PVDF) syringe filter. HPLC analysis was performed with an Agilent 1100 HPLC system equipped with Ascentis C18 column (25 cm × 4.6 mm, particle size: 5 µm). The mobile phase was a 50:50 volume mixture of water and ACN and run at 1 mL min^{-1}. PTX was detected by a UV detector at a wavelength of 227 nm. Drug loading efficiency was defined as the PTX amount divided by the NP mass.

PTX Release Kinetics: NPs equivalent to 10 µg of PTX were suspended in 1 mL of PBS containing 0.2% Tween 20 and incubated at 37 °C under constant agitation. At timed intervals, NP suspension was ultracentrifuged at 34 000× g for 15 min. 0.8 mL of supernatant was sampled for HPLC analysis and replaced with 0.8 mL of fresh release medium. NPs were resuspended in the medium by brief ultrasonication and returned to incubation.

Cell Culture: HUVECs (ATCC, Manassas, VA, USA) at passage 4 were grown in EGM-2 complete medium. Culture plates were precoated with 5 µg cm^{-2} of rat tail collagen type I. Human breast adenocarcinoma cells (MDA-MB-231, ATCC; MCF-7, ATCC) were cultured in DMEM supplemented with 10% FBS. Human colon adenocarcinoma cells (LS174T, ATCC) were cultured in EMEM supplemented with 10% FBS. Human ovarian cancer cells (A2780, ATCC) were cultured in RPMI supplemented with 10% FBS. Human ovarian cancer cells (NCI/ADR-RES) were cultured in DMEM supplemented with 10% FBS. Mouse hemangioendothelioma cells (EOMA, ATCC) were cultured in DMEM supplemented with 10% FBS. Mouse mammary carcinoma cells (4T1, ATCC) were cultured in RPMI supplemented with 10% FBS. Mouse melanoma cells (B16F10, ATCC) were cultured in RPMI supplemented with 10% FBS. Mouse monocyte macrophages (J774A.1, ATCC) were cultured in DMEM supplemented with 10% FBS. All media were supplemented with 100 units mL^{-1} penicillin and 100 µg mL^{-1} streptomycin. All cells were subcultured at a ratio of 1:7.5 when they became 70–80% confluent. HUVECs was used between 4 and 7 passages, and all other cells were used in less than 20 passages.

Cytotoxicity of QA-NH_2 on HUVECs: HUVECs were seeded in a 96 well plate at a density of 10 000 cells per well coated with rat tail collagen type I. A group of cells were incubated with 10 ng mL^{-1} of TNF-α for 4 h and then treated with QA-NH_2 (1×10^{-9} M to 1×10^{-3} M) for 24 h.

The cell viability was determined by the MTT (3-(4,5-dimethylthiazol-2-yl)-2,5-diphenyltetrazolium bromide) assay. Cells were treated with 75 µg of MTT and incubated for 4 h. The formazan crystals were dissolved in stop/solubilization solution (50% DMF, 20% sodium dodecyl sulfate (SDS), pH 5) and quantified by a SpectraMax M3 microplate reader (Molecular Devices, CA, USA) at the wavelength of 562 nm. The measured absorbance was normalized to the absorbance of control cells that did not receive any treatment.

Cytotoxicity of PTX@QA-NP on MDA-MB-231 Cells: MDA-MB-231 cells were seeded in a 96 well plate at a density of 10 000 cells per well. After overnight incubation, the culture medium was replaced with fresh DMEM, to which PTX, PTX + QA-NP, and PTX@QA-NP were added to provide the final PTX concentration ranging from 0.1×10^{-9} M to 100×10^{-6} M. After 72 h incubation, the cell viability was determined by the MTT assay.

Confocal Microscopy of In Vitro NP–Cell Interactions: HUVECs were seeded in a 35 mm dish with a glass window (MatTek Corporation, Ashland, MA, USA) coated with rat tail collagen type I and grown in EGM-2 complete medium. When HUVECs were 80% confluent, cells were treated with 10 ng mL^{-1} of TNF-α for 4 h. The medium was replaced with EGM-2 containing 0.2 mg mL^{-1} of FITC-labeled NP suspension and incubated for 2 h at 37 °C. The suspension was replaced with fresh EGM-2 medium containing 0.5×10^{-6} M CellMask deep red membrane staining dye. After 10 min, cells were gently rinsed with PBS twice. Hoechst nuclear stain (10 µL at the concentration of 0.2 mg mL^{-1}) was added 10 min prior to the imaging. Imaging was performed with a Nikon A1R confocal microscope (Melville, NT, USA) equipped with a Spectra Physics 163C argon ion laser and a Coherent CUBE diode laser. The NPs, cell nuclei, and cell membrane were excited using 495, 361, and 649 nm laser, respectively, and detected at 519, 497, and 666 nm.

Flow Cytometry for Quantitative Analysis of NP–Cell Interactions: For quantitative analysis of NP–cell interaction, HUVECs were treated with FITC-labeled NPs in the same way as confocal microscopy and gently washed with PBS twice to remove free or loosely bound NPs. The cells were then trypsinized, collected by centrifugation at 930× g for 5 min, resuspended in 0.2 mL of PBS at 4 °C, and analyzed by an Accuri C6 flow cytometer (BD Biosciences, San Jose, CA, USA) equipped with an FL-1 detector ($\lambda_{ex}/\lambda_{em}$ = 488/525 nm).

For competition assay, free QA-NH_2, E-selectin antibody, or P-selectin antibody were preincubated with HUVECs for 30 min prior to the NP treatment and flow cytometry analysis. In another competition assay, known concentrations of NP, NP (PLGA–$TPGS_{5k}$), QA-NP, and QA-NP (PLGA–$TPGS_{5k}$) were preincubated with the activated HUVECs for 30 min. The pretreated HUVECs were incubated with FITC-labeled QA-NP for 2 h and analyzed by flow cytometry.

Macrophage interactions of bare NP and QA-NP were compared. J774A.1 macrophages were seeded at a density of 100 000 cells cm^{-2} in a 6-well plate. When 70–80% confluent, the cells were incubated with 0.1 mg mL^{-1} of FITC-labeled QA-NP, NP, or NP-pD at an equivalent fluorescence level in DMEM and incubated for 2 h at 37 °C. The cells were washed with PBS twice and analyzed by flow cytometry.

Transendothelial NP Transport Across Confluent HUVECs: HUVECs were seeded in a Corning Transwell insert coated with rat tail collagen type I and grown in EGM-2 complete medium. The TEER across the HUVEC layer in the Transwell insert was monitored daily by EVOM2 epithelial voltohmmeter (World Precision Instruments, Sarasota, FL, USA). When the TEER value reached a plateau (indicating confluency), the HUVEC layer was treated with 10 ng mL^{-1} of TNF-α for 4 h, followed by incubation with 0.1 mg mL^{-1} of FITC-labeled NP or QA-NP for 8 h. The fluorescence intensity of total NPs prior to incubation and those of NPs in the apical and basolateral sides of a Transwell insert after incubation period were measured by FluoroMax-3 spectrofluorometer (Horiba Scientific, Edison, NJ, USA). In a separate study, the confluent, TNF-α activated HUVECs were treated with 0.1 mg mL^{-1} of NP or QA-NP for 8 h, followed by 16 h incubation in NP-free medium. The TEER values were measured at 0, 4, 8, 12, and 24 h from the NP treatment.

Endothelial Expression of E-Selectin and P-Selectin by Tumor-Conditioned Media—Human Cell Lines: HUVECs were seeded in a 6-well plate coated with rat tail collagen type I at a density of 10 000 cells cm^{-2}. When HUVECs became 70–80% confluent, cells were exposed to the culture media conditioned with MCF-7, MDA-MB-231, LS174T, A2780, or NCI-ADR cells for 4 h. Respective cell-free media were used as medium controls, and TNF-α (10 ng mL^{-1}) was used as a positive control. The HUVECs were trypsinized and collected via centrifugation. The cell pellets were resuspended in PBS and stained with FITC-labeled anti-human E-selectin or anti-human P-selectin antibody according to the manufacturer's protocol. The extent of E-selectin or P-selectin expressions was quantified by flow cytometry.

Mouse Cell Lines: EOMAs at passage 2 were seeded in a 6-well plate at a density of 10 000 cells cm^{-2}. When EOMAs became 70–80% confluent, cells were exposed to the culture media conditioned with 4T1 or B16F10 cells for 4 h. Respective cell-free media were used as medium controls, and TNF-α (10 ng mL^{-1}) and lipopolysaccharide (O111:B4 from *E. coli*, 10 ng mL^{-1}) were used as positive controls. EOMAs were collected in the same way as above, stained with FITC-labeled anti-mouse E-selectin or anti-mouse P-selectin antibody, and analyzed by flow cytometry.

Immunohistochemistry of E-/P-Selectin Expression in MDA-MB-231 Xenograft Model: MDA-MB-231 xenograft tumors were fixed in formalin and embedded in paraffin blocks. The tissue blocks were cut in 3 µm thick sections, deparaffinized by xylene, and treated with 0.3% hydrogen peroxide and the antigen retrieval buffer (10×10^{-3} M Tris, 1×10^{-3} M ethylenediaminetetraacetic acid (EDTA), 0.03% Tween 20). The sections were blocked with PBS containing 4% bovine serum albumin (BSA) and 0.03% Tween 20. The sections were incubated with anti-E-selectin antibody (1:800 dilution, AF575, R&D system) and anti-P-selectin antibody (1:200 dilution, AF737, R&D system) for 1 h, followed by corresponding secondary antibodies conjugated with horse peroxidase (One-step or Two-step Polymer Detection Systems, Nichirei, Japan). The selectin signals were visualized by incubation with 3, 3′-diaminobenzidine (DAB) for 7 min. The sections were counterstained with hematoxylin and imaged with an Eclipse 80i microscope (Nikon, Japan).

Confocal Imaging of QA-NP Accumulation in X-Irradiated Tumor: Balb/c female mice (6–8 weeks old) were purchased from Envigo (Indianapolis, IN, USA). All mice were maintained under pathogen-free conditions. The study was approved by the Institutional Animal Care and Use Committee of the University of Chicago, and all experiments conformed to the relevant regulatory standards. CT26 cells (ATCC CRL-2638) were cultured in 5% CO_2 and maintained in DMEM supplemented with 10% heat-inactivated fetal bovine serum, 2×10^{-3} M L-glutamine, and 100 units mL^{-1} penicillin. To form subcutaneous tumors, 5×10^5 CT26 cells were injected into both hind limbs of a mouse. Ten days after tumor implantation, CT26 tumor on the right hind limb was X-irradiated with 6 Gy using an X-RAD 225 Cx image-guided radiotherapy system (Precision X-Ray) at 225 kV, 13 mV, 1.1 mm Cu half-value layer, and a dose rate of 2.5 Gy min^{-1}. At 2 days after radiation, DyLight 594-labeled QA-NP or PEG-NP (1 mg in 0.2 mL PBS) solution was IV injected to the mouse. At 1 day postinjection of NPs, CT26 tumors were harvested, washed with cold PBS, fixed with 2% paraformaldehyde in PBS for 10 min at room temperature, and washed with PBS. The washed tumors were cast in 2% agarose gel (dissolved in distilled water, LE Quick Dissolve Agarose, GeneMate) in 24 well plates. The gel plugs containing tumors were mounted on a vibrating microtome (VT1200S, Leica) equipped with a buffer tray. Sections (in 0.4 mm thickness) were collected in order in cold PBS. The macrosections were stained with DyLight 488-anti-F4/80 (BioXcell, clone CI:A3-1), DyLight 550-anti-E-selectin (BioLegend, clone RME-1/CD62E), DyLight 633-anti-CD31 (BioLegend, clone MEC13.3), and DyLight 680-anti-P-selectin (BioLegend, clone RMP-1) antibodies in staining buffer (SB, RPMI 1640 media with 10 mg mL^{-1} BSA and 0.1% Triton X-100) at 4 °C overnight. The macrosections were incubated in 10 mL of 80% D-fructose solution for 1 h at 25 °C with gentle agitation. The stained sections were imaged by a Leica TCS SP8 confocal laser scanning microscope, equipped with a white light laser, a HC PL APO 40X/1.25 NA oil objective (0.24 mm working distance), 488 nm excitation and 495–528 nm emission filter for DyLight 488, 550 nm excitation and 563–579 nm emission filter for DyLight 550, 594 nm excitation and 600–620 nm filters for DyLight 594, 633 nm excitation and 637–655 nm filter for DyLight 633, and 670 nm excitation and 680–700 nm filter for DyLight 680.

Whole Body Imaging: Female athymic nude mice (Foxn1^{nu}) at the age of 6–7 weeks were purchased from Envigo (Indianapolis, IN, USA) and acclimatized for 3 days prior to the procedure. All animal procedures were approved by the Purdue Animal Care and Use Committee, in compliance with the NIH guidelines for the care and use of laboratory animals. Each mouse received 5×10^6 MDA-MB-231 cells in the flank of hind leg by subcutaneous injection. When the average tumor volume reached 200 mm^3, each mouse received 6 mg of ICG-labeled QA-NP or PEG-NP in 0.9% saline via tail vein injection. The animals were imaged with an IVIS Lumina II system (Caliper Life Sciences, Hopkinton, MA, USA) to detect near infrared fluorescence signal of ICG over 24 h. After 24 h, mice were sacrificed, and tumors and major organs were retrieved and imaged with the IVIS Lumina system. The experiment was repeated with another set of tumor-bearing animals receiving 6 mg of ICG-labeled QA-NP or PEG-NP in 0.9% saline via tail vein injection. The image of ex vivo organs was taken at 6 h postinjection using the IVIS Lumina system.

Intravital Microscopy: Female Balb/c nude mice at the age of 8 weeks were purchased from OrientBio (Suwon, Korea). All animal experiments were performed in accordance with the standard guidelines for the care and use of laboratory animals as approved by the Institutional Animal Care and Use Committee of KAIST (protocol no. KA2013-30). All surgeries were performed under anesthesia. A dorsal skinfold chamber was implanted into a mouse.[53] Immediately after the implantation, a mixture of 3×10^6 MDA-MB-231-GFP cells and Corning Matrigel matrix was injected to the center of a dorsal skinfold window chamber. After 1 week from the implantation, intravital imaging was performed. Two milligrams of Alexa Fluor 555-labeled QA-NP was IV injected via tail vein through a custom-built catheter composed of 30 gauge needle tip and a polyethylene tube. At 2, 6, and 24 h after the NP injection, tumor microenvironment was repeatedly visualized to locate the NPs. At 3 h before intravital imaging, 25 µg of anti-CD31 monoclonal antibody (553 370, BD) conjugated to Alexa Fluor 647 (A20106, Invitrogen) was IV injected to label the blood vessels. For P-selectin (CD62P) or E-selectin (CD62E) labeling, 25 µg of anti-P-selectin monoclonal antibody (553742, BD) or anti-E-selectin monoclonal antibody (553749, BD) conjugated to Alexa Fluor 647 (A20106, Invitrogen) was IV injected at 3 h before the intravital imaging. During intravital imaging, the body temperature of the mouse was continuously monitored and maintained at 37 °C by the homeothermic system (RightTemp, Kent Scientific).

A custom-built video-rate laser-scanning confocal microscopy system[54] was used for intravital imaging. Three laser modules with output wavelengths at 488 nm (MLD488, Cobolt), 561 nm (Jive, Cobolt), and 640 nm (MLD640, Cobolt) were used as excitation light sources. Three photomultiplier tubes (R9110, Hamamatsu) with bandpass filters (FF02-525/50, FF01-600/37, FF01-685/40, Semrock) were used for multicolor confocal fluorescence imaging. To achieve 2D laser beam scanning at video-rate of 30 Hz, a rapidly rotating polygonal mirror with 36 facets (MC-5, aluminum coated, Lincoln Laser) for *x*-axis scanning and a galvanometer scanning mirror (6230H, Cambridge Technology) for *y*-axis scanning were used. A commercial objective lens (CFI Plan Apo lambda, 20X, NA 0.75, Nikon) was used to capture confocal fluorescence images.

Determination of Maximum Tolerated Dose of PTX@QA-NP: Female athymic nude mice (Foxn1^{nu}) at the age of 6–7 weeks were administered with PTX@QA-NP varying the frequency of the dosing. Each time, animals received the NPs at a PTX dose of 30 mg kg^{-1} through tail vein injection and monitored over 15 days. The body weight was measured every other day. Weight loss in excess of 20% was considered a humane endpoint.

In Vivo Anticancer Efficacy: Female athymic nude mice (Foxn1^{nu}) at the age of 6–7 weeks received 5×10^6 MDA-MB-231 cells in the flank of hind leg by subcutaneous injection. When the averaged tumor volume reached 100 mm^3, each mouse received saline, bare QA-NP, bare PEG-NP, PTX@PEG-NP, or PTX@QA-NP at a dose equivalent to 30 mg kg^{-1} PTX 10 times over a 2-week period via tail vein injection. The tumor volume was measured every other day. The length (L) and width (W) of each tumor were measured by a digital caliper, and the volume (V) was calculated by the modified ellipsoid formula: $V = (L \times W^2)/2$.[55] Specific growth rate of a tumor was calculated as $\Delta \log V/\Delta t$ (t: time in days).[56] Mice with ulcerated tumors or tumors greater than 2000 mm^3 were euthanized in a humane manner. Two other sets of experiments were carried out to compare PTX@QA-NP with Taxol: One group received a single dose at 20 mg kg^{-1} PTX equivalent, and the other received 5 doses of 20 mg kg^{-1} PTX equivalent every 3 days over 2 weeks.

Male C57BL/6 mice at the age of 5–6 weeks were purchased from Envigo (Indianapolis, IN, USA) and acclimatized for 3 days prior to the procedure. Each mouse received 5×10^6 B16F10 cells in the flank of hind leg by subcutaneous injection. When the averaged tumor volume reached 100 mm^3, each mouse received a single dose of PTX@QA-NP or Taxol at 20 mg kg^{-1} PTX equivalent and was monitored in the same way as above.

Comparison of Tumor Vascularization: Female athymic nude mice (Foxn1^{nu}) at the age of 6–7 weeks received 5×10^6 MDA-MB-231 cells or LS174T cells in the flank of hind leg by subcutaneous injection. When the averaged tumor volume reached 200 mm^3, 200 µL of 0.25% Evans blue (Abcam, Cambridge, UK) in PBS was injected via tail vein. After 1 h, the mice were sacrificed, and the tumors and muscle tissues were imaged.

Detection of Anti-PEG Antibody in NP-Treated Animals: Female athymic nude mice (Foxn1^{nu}) at the age of 6–7 weeks received tail-vein injection of saline or PEG-NP or QA-NP (30 mg kg^{-1}). Five days later, blood was obtained by cardiac puncture and collected in a BD Vacutainer Plus Plastic Serum Tube. Serum was separated by centrifugation at 930× g for 15 min. In the meantime, 200 µL of 2 mg mL^{-1} dopamine Tris solution was added to each well of a 96-well plate for surface coating. After 4 h incubation at room temperature, the plate was triple rinsed with DI water and incubated with 200 µL of 2 mg mL^{-1} mPEG-NH_2 or QA-NH_2 for each ligand decoration. After 1 h, the plate was triple rinsed with DI water and treated with 100 µL of 1% human serum albumin (HSA) blocking buffer (Tris buffered saline + 1% HSA + 0.05% Tween 20) for 1 h, followed by quintuple rinse. The blocked well was incubated with 100 µL of diluted sera from the NP-treated animals (1:20 dilution) for 1 h and rinsed 5 times. Goat anti-mouse IgM IgG-HRP conjugate (0.8 or 4 µg mL^{-1}) was added to each well for 1 h incubation followed by quintuple rinse. Another 100 µL of 1% HSA blocking buffer was added to each well for 1 h incubation and rinsed 5 times. Finally, each well was treated with 50 µL of 3,3′,5,5′-tetramethylbenzidine for 5 min to develop a blue color corresponding to the amount of the bound IgG-HRP, followed by quenching with 2 M sulfonic acid. The substrate solution was transferred to another plate for absorbance measurement at 450 nm.

PK and Biodistribution of PTX: Female athymic nude mice (Foxn1^{nu}) at the age of 6–7 weeks were inoculated with 5×10^6 MDA-MB-231 cells in the flank of hind leg by subcutaneous injection. When the average tumor size reached 100 mm^3, animals were administered with PTX@PEG-NP, PTX@QA-NP, and Taxol at a PTX dose of 20 mg kg^{-1} by tail vein injection. At predetermined time points, 3 mice were randomly sacrificed for the collection of blood and major organs. Blood was obtained by cardiac puncture and collected in a BD Vacutainer PST tube. Plasma was separated from whole blood via centrifugation at 3000× g for 15 min.

Plasma and tissue concentrations of PTX were quantified using docetaxel (DTX) as the internal standard. Samples were prepared by liquid–liquid extraction. Specifically, plasma samples were diluted with water and extracted with methyl tertiary butyl ether. The samples were mixed and spun at high speed. The organic layer was transferred to a tube, evaporated to dryness, the tube was reconstituted with methanol, and a small volume was injected into the HPLC-MS/MS. For tissues samples, frozen tissue was weighed, phosphate buffer (100×10^{-3} M, pH 7.4) was added, and the tissue was homogenized using a Qiagen TissueRuptor with disposable probes. A volume of homogenate was removed, internal standard added, and the tissue sample was extracted using the same procedure that was used for plasma. Standards containing known amounts of PTX were prepared to estimate the concentrations in the samples. The standards ranged from 0.1–1000 ng mL^{-1} (n = 10 standards including a 0) for mouse plasma samples. The

standards ranged from 0.8 to 80 ng per sample (n = 6 including a 0) for tumor, spleen, lung, kidney, and heart tissues, and from 1.8 to 180 ng per sample (n = 6 including a 0) for liver tissue. The tissues from mice receiving no treatment were used as the matrix in the standard preparation for the respective tissues. The samples were analyzed by HPLC-MS/MS (ABSciex 4000). The mass spectrometer utilized an electrospray ionization probe and was run in positive mode. The multiple reaction monitoring Q1/Q3 (m/z) transitions were 854.3/286.0 and 808.2/527.1, for PTX and DTX respectively.

The PK parameters were obtained via noncompartmental analyses using the sparse data option of WinNonlin (version 7.0, Certara, NJ, USA), allowing for the computation of the standard errors (SE) associated with estimated parameters.

Statistical Analysis: All statistical analysis was performed with GraphPad Prism 7 (La Jolla, CA, USA). All data were analyzed with one-way or two-way ANOVA test to determine the statistical difference of means among various groups, followed by the recommended multiple comparisons tests. A p-value less than 0.05 was considered statistically significant.

Supporting Information

Supporting Information is available from the Wiley Online Library or from the author.

Acknowledgements

This work was supported by the National Institutes of Health NIBIB R01EB017791, the Lilly Endowment Gift Graduate Research Award (J.X.), and NIBIB K99 EB022636 (S.S.-Y.L.). This work was also supported by the Purdue Research Foundation and the Indiana Clinical and Translational Sciences Institute, funded in part by grant #UL1 TR001108 from the National Institutes of Health, National Center for Advancing Translational Sciences, Clinical and Translational Sciences Award. HPLC-MS/MS analysis was performed by the Clinical Pharmacology Analytical Core laboratory, a core laboratory of the Indiana University Melvin and Bren Simon Cancer Center supported by the National Cancer Institute grant P30 CA082709. The authors thank Samyang Biopharm (Seoul, Korea) for the kind donation of paclitaxel and Prof. You-Yeon Won and Hyun Chang Kim for the assistance with PLGA–TPGS synthesis.

Conflict of Interest

The authors declare no conflict of interest.

Keywords

drug delivery, polymeric nanoparticles, quinic acid, selectin, tumor microenvironment

Received: September 3, 2018
Revised: October 11, 2018
Published online:

[1] a) D. Peer, J. Karp, S. Hong, O. C. Farokhzad, R. Margalit, R. Langer, *Nat. Nanotechnol.* **2007**, *2*, 751; b) J. Shi, P. W. Kantoff, R. Wooster, O. C. Farokhzad, *Nat. Rev. Cancer* **2017**, *17*, 20.
[2] Y. Matsumura, H. Maeda, *Cancer Res.* **1986**, *46*, 6387.
[3] S. Wilhelm, A. J. Tavares, Q. Dai, S. Ohta, J. Audet, H. F. Dvorak, W. C. W. Chan, *Nat. Rev. Mater.* **2016**, *1*, 1
[4] H. Ledford, *Nature* **2016**, *533*, 304.
[5] a) E. Karathanasis, L. Chan, L. Karumbaiah, K. McNeeley, C. J. D'Orsi, A. V. Annapragada, I. Sechopoulos, R. V. Bellamkonda, *PLoS One* **2009**, *4*, e5843; b) H. Maeda, *Adv. Drug Delivery Rev.* **2015**, *91*, 3.
[6] a) G. S. Kansas, *Blood* **1996**, *88*, 3259; b) M. B. Lawrence, T. A. Springer, *Cell* **1991**, *65*, 859.
[7] a) H. Laubli, L. Borsig, *Semin. Cancer Biol.* **2010**, *20*, 169; b) N. Makrilia, A. Kollias, L. Manolopoulos, K. Syrigos, *Cancer Invest.* **2009**, *27*, 1023.
[8] a) M. Nguyen, N. A. Strubel, J. Bischoff, *Nature* **1993**, *365*, 267; b) A. E. Koch, M. M. Halloran, C. J. Haskell, M. R. Shah, P. J. Polverini, *Nature* **1995**, *376*, 517.
[9] S. R. Barthel, J. D. Gavino, L. Descheny, C. J. Dimitroff, *Expert Opin. Ther. Targets* **2007**, *11*, 1473.
[10] a) P. Gassmann, A. Enns, J. Haier, *Onkologie* **2004**, *27*, 577; b) H. Kobayashi, K. C. Boelte, P. C. Lin, *Curr. Med. Chem.* **2007**, *14*, 377; c) G. E. Rice, M. P. Bevilacqua, *Science* **1989**, *246*, 1303; d) Z. J. Liu, R. Tian, Y. Li, W. An, Y. Zhuge, A. S. Livingstone, O. C. Velazquez, *Ann. Surg.* **2011**, *254*, 450.
[11] M. P. Bevilacqua, R. M. Nelson, *J. Clin. Invest.* **1993**, *91*, 379.
[12] a) B. F. R. Bonfanti, B. Furie, D. D. Wagner, *Blood* **1989**, *73*, 1109; b) D. E. Hallahan, S. Virudachalam, *Radiat. Res.* **1999**, *152*, 6.
[13] L. J. Gay, B. Felding-Habermann, *Nat. Rev. Cancer* **2011**, *11*, 123.
[14] Y. Shamay, M. Elkabets, H. Li, J. Shah, S. Brook, F. Wang, K. Adler, E. Baut, M. Scaltriti, P. V. Jena, E. E. Gardner, J. T. Poirier, C. M. Rudin, J. Baselga, A. Haimovitz-Friedman, D. A. Heller, *Sci. Transl. Med.* **2016**, *8*, 345ra87.
[15] a) M. Nguyen, C. L. Corless, B. M. Kraling, C. Tran, T. Atha, J. Bischoff, S. H. Barsky, *Am. J. Pathol.* **1997**, *150*, 1307; b) O. G. Shaker, M. A. A. El-Deen, M. T. A. El-Rahim, R. M. Talaat, *Tumori* **2006**, *92*, 524; c) S. B. Fox, G. D. Turner, K. C. Gatter, A. L. Harris, *J. Pathol.* **1995**, *177*, 369.
[16] B. Hemmerlein, J. Scherbening, A. Kugler, H. J. Radzun, *Histopathology* **2000**, *37*, 78.
[17] a) L. B. Young, J. Kim, N. M. Varki, A. Varki, *Proc. Natl. Acad. Sci. USA* **1998**, *95*, 9325; b) L. Gong, H. J. Mi, H. Zhu, X. Zhou, H. Yang, *Mol. Med. Rep.* **2012**, *5*, 935.
[18] M. Mollà, M. Gironella, A. Salas, R. Miquel, S. Pérez-del-Pulgar, C. Conill, P. Engel, A. Biete, J. M. Piqué, J. Panés, *Int. J. Cancer* **2001**, *96*, 99.
[19] M. Phillips, E. Nudelman, F. Gaeta, M. Perez, A. Singhal, S. Hakomori, J. Paulson, *Science* **1990**, *250*, 1130.
[20] a) S. Pedatella, M. De Nisco, B. Ernst, A. Guaragna, B. Wagner, R. J. Woods, G. Palumbo, *Carbohydr. Res.* **2008**, *343*, 31; b) I. Robina, A. Moreno-Vargas, A. Carmona, A. Ferrali, L. Molina, presented at *Abstracts of Papers, 233rd ACS National Meeting*, Chicago, IL, USA, March **2007**; c) H. Huang, C.-H. Wong, *J. Org. Chem.* **1995**, *60*, 3100; d) B. N. Rao, M. B. Anderson, J. H. Musser, J. H. Gilbert, M. E. Schaefer, C. Foxall, B. K. Brandley, *J. Biol. Chem.* **1994**, *269*, 19663; e) M. W. Cappi, W. J. Moree, L. Qiao, T. G. Marron, G. Weitz-Schmidt, C.-H. Wong, *Bioorg. Med. Chem.* **1997**, *5*, 283; f) S. A. DeFrees, L. Phillips, L. Guo, S. Zalipsky, *J. Am. Chem. Soc.* **1996**, *118*, 6101; g) N. Kaila, B. E. ThomasIV, *Med. Res. Rev.* **2002**, *22*, 566; h) N. Kaila, *J. Med. Chem.* **2005**, *48*, 4346.
[21] a) R. Zeisig, R. Stahn, K. Wenzel, D. Behrens, I. Fichtner, *Biochim. Biophys. Acta, Biomembr.* **2004**, *1660*, 31; b) Y. Shamay, L. Raviv, M. Golan, E. Voronov, R. N. Apte, A. David, *J. Controlled Release* **2015**, *217*, 102.
[22] a) C. Girard, J. Dourlat, A. Savarin, C. Surcin, S. Leue, V. Escriou, C. Largeau, J. Herscovici, D. Scherman, *Bioorg. Med. Chem. Lett.* **2005**, *15*, 3224; b) Y. Shamay, D. Paulin, G. Ashkenasy, A. David, *J. Med. Chem.* **2009**, *52*, 5906.
[23] a) Z. Amoozgar, J. Park, Q. Lin, J. H. Weidle3rd, Y. Yeo, *Biomacromolecules* **2013**, *14*, 2389; b) Y. Shamay, D. Paulin, G. Ashkenasy, A. David, *Biomaterials* **2009**, *30*, 6460.

[24] Y. Liu, R. Zhong, P. Zhang, Y. Ma, X. Yun, P. Gong, J. Wei, X. Zhao, F. Zhang, *ACS Appl. Mater. Interfaces* **2016**, *8*, 2478.
[25] W. Rao, H. Wang, J. Han, S. Zhao, J. Dumbleton, P. Agarwal, W. Zhang, G. Zhao, J. Yu, D. L. Zynger, X. Lu, X. He, *ACS Nano* **2015**, *9*, 5725.
[26] J. Park, T. F. Brust, H. J. Lee, S. C. Lee, V. J. Watts, Y. Yeo, *ACS Nano* **2014**, *8*, 3347.
[27] H. Lee, W. M. Miller, P. B. Messersmith, *Science* **2007**, *318*, 426.
[28] H. Lee, J. Rho, P. B. Messersmith, *Adv. Mater.* **2009**, *21*, 431.
[29] a) N. Peyri, M. Berard, F. Fauvel-Lafeve, V. Trochon, B. Arbeille, H. Lu, C. Legrand, M. Crepin, *Anticancer Res.* **2009**, *29*, 2347; b) H. Shoval, A. Karsch-Bluman, Y. Brill-Karniely, T. Stern, G. Zamir, A. Hubert, O. Benny, *Sci. Rep.* **2017**, *7*, 10428; c) E. Lee, N. B. Pandey, A. S. Popel, *Sci. Rep.* **2015**, *4*, 5853.
[30] a) C. J. Stocker, K. L. Sugars, O. A. Harari, R. C. Landis, B. J. Morley, D. O. Haskard, *J. Immunol.* **2000**, *164*, 3309; b) V. Bhaskar, D. A. Law, E. Ibsen, D. Breinberg, K. M. Cass, R. B. DuBridge, F. Evangelista, S. M. Henshall, P. Hevezi, J. C. Miller, M. Pong, R. Powers, P. Senter, D. Stockett, R. L. Sutherland, U. von Freeden-Jeffry, D. Willhite, R. Murray, D. E. Afar, V. Ramakrishnan, *Cancer Res.* **2003**, *63*, 6387; c) Y. Lu, T. Yu, H. Liang, J. Wang, J. Xie, J. Shao, Y. Gao, S. Yu, S. Chen, L. Wang, L. Jia, *Sci. Rep.* **2015**, *4*, 4344; d) S. Magder, J. Neculcea, V. Neculcea, R. Sladek, *J. Vasc. Res.* **2006**, *43*, 447.
[31] a) E. O. Harrington, T. Stefanec, J. Newton, S. Rounds, *Lung* **2006**, *184*, 259; b) . J. F. Leeuwenberg, E. F. Smeets, J. J. Neefjes, M. A. Shaffer, T. Cinek, T. M. Jeunhomme, T. J. Ahern, W. A. Buurman, *Immunology* **1992**, *77*, 543.
[32] a) L. Zhong, B. Simoneau, J. Huot, M. J. Simard, *Oncotarget* **2017**, *8*, 1678; b) J. Laferriere, F. Houle, J. Hout, *Ann. N. Y. Acad. Sci.* **2002**, *973*, 562.
[33] a) P. L. Tremblay, F. A. Auger, J. Huot, *Oncogene* **2006**, *25*, 6563; b) P. Khanna, T. Yunkunis, H. S. Muddana, H. H. Peng, A. August, C. Dong, *Am. J. Physiol.: Cell Physiol.* **2010**, *298*, C1140.
[34] T. Nubel, W. Dippold, B. Kaina, G. Fritz, *Carcinogenesis* **2004**, *25*, 1335.
[35] S. S. Lee, V. P. Bindokas, S. J. Kron, *Sci. Rep.* **2017**, *7*, 17031.
[36] Q. Wu, A. Allouch, I. Martins, N. Modjtahedi, E. Deutsch, J. L. Perfettini, *Biomed. J.* **2017**, *40*, 200.
[37] M. A. Miller, R. Chandra, M. F. Cuccarese, C. Pfirschke, C. Engblom, S. Stapleton, U. Adhikary, R. H. Kohler, J. F. Mohan, M. J. Pittet, R. Weissleder, *Sci. Transl. Med.* **2017**, *9*, eaal0225.
[38] G. Hariri, Y. Zhang, A. Fu, Z. Han, M. Brechbiel, M. N. Tantawy, T. E. Peterson, R. Mernaugh, D. Hallahan, *Ann. Biomed. Eng.* **2008**, *36*, 821.
[39] E. F. Smeets, T. De Vries, J. F. M. Leeuwenberg, D. H. van den Eijnden, W. A. Buurman, J. J. Neefjes, *Eur. J. Immunol.* **1993**, *23*, 147.
[40] J. J. Chiu, L. J. Chen, C. I. Lee, P. L. Lee, D. Y. Lee, M. C. Tsai, C. W. Lin, S. Usami, S. Chien, *Blood* **2007**, *110*, 519.
[41] a) T. Desmettre, J. M. Devoisselle, S. Mordon, *Surv. Ophthalmol.* **2000**, *45*, 15; b) M. A. Yaseen, J. Yu, B. Jung, M. S. Wong, B. Anvari, *Mol. Pharmaceutics* **2009**, *6*, 1321.
[42] P. A. Jarzyna, L. H. Deddens, B. H. Kann, S. Ramachandran, C. Calcagno, W. Chen, A. Gianella, R. M. Dijkhuizen, A. W. Griffioen, Z. A. Fayad, W. J. M. Mulder, *Neoplasia* **2012**, *14*, 964.
[43] H. Bumpers, M. B. Huang, V. Katkoori, U. Manne, V. Bond, *J. Cancer Ther.* **2013**, *04*, 898.
[44] a) H. Cabral, Y. Matsumoto, K. Mizuno, Q. Chen, M. Murakami, M. Kimura, Y. Terada, M. R. Kano, K. Miyazono, M. Uesaka, N. Nishiyama, K. Kataoka, *Nat. Nanotechnol.* **2011**, *6*, 815; b) H. Lee, H. Fonge, B. Hoang, R. M. Reilly, C. Allen, *Mol. Pharmaceutics* **2010**, *7*, 1195; c) L. Tang, X. Yang, Q. Yin, K. Cai, H. Wang, I. Chaudhury, C. Yao, Q. Zhou, M. Kwon, J. A. Hartman, I. T. Dobrucki, L. W. Dobrucki, L. B. Borst, S. Lezmi, W. G. Helferich, A. L. Ferguson, T. M. Fan, J. Cheng, *Proc. Natl. Acad. Sci. USA* **2014**, *111*, 15344.
[45] Y.-L. Su, T.-W. Yu, W.-H. Chiang, H.-C. Chiu, C.-H. Chang, C.-S. Chiang, S.-H. Hu, *Adv. Funct. Mater.* **2017**, *27*, 1700056.
[46] S. A. Abouelmagd, Y. J. Ku, Y. Yeo, *J. Drug Targeting* **2015**, *23*, 725.
[47] Y. Ma, Y. Zheng, K. Liu, G. Tian, Y. Tian, L. Xu, F. Yan, L. Huang, L. Mei, *Nanoscale Res. Lett.* **2010**, *5*, 1161.
[48] X. Zhang, H. M. Burt, G. Mangold, D. Dexter, D. Von Hoff, L. Mayer, W. L. Hunter, *Anti-Cancer Drugs* **1997**, *8*, 696.
[49] W. Willem, N. P. R. Overwijk, *Curr. Protoc. Immunol.* **2001**, *20.1*, 1.
[50] a) Y. Mima, Y. Hashimoto, T. Shimizu, H. Kiwada, T. Ishida, *Mol. Pharmaceutics* **2015**, *12*, 2429; b) T. Ishida, R. Maeda, M. Ichihara, K. Irimura, H. Kiwada, *J. Controlled Release* **2003**, *88*, 35; c) T. Ishida, K. Masuda, T. Ichikawa, M. Ichihara, K. Irimura, H. Kiwada, *Int. J. Pharm.* **2003**, *255*, 167; d) T. Ishida, M. Ichihara, X. Wang, H. Kiwada, *J. Controlled Release* **2006**, *115*, 243; e) T. Ishida, M. Ichihara, X. Wang, K. Yamamoto, J. Kimura, E. Majima, H. Kiwada, *J. Controlled Release* **2006**, *112*, 15; f) T. Ishida, K. Atobe, X. Wang, H. Kiwada, *J. Controlled Release* **2006**, *115*, 251.
[51] A. S. Abu Lila, H. Kiwada, T. Ishida, *J. Controlled Release* **2013**, *172*, 38.
[52] a) J. Spratlin, M. B. Sawyer, *Crit. Rev. Oncol./Hematol.* **2007**, *61*, 222; b) B. Monsarrat, E. Mariel, S. Cros, M. Garès, D. Guénard, F. Guéritte-Voegelein, M. Wright, *Drug Metab. Dispos.* **1990**, *18*, 895; c) V. R. Panday, M. T. Huizing, P. H. Willemse, A. De Graeff, W. W. ten Bokkel Huinink, J. B. Vermorken, J. H. Beijnen, *Semin. Oncol.* **1997**, *24*, S11; d) B. Monsarrat, P. Alvinerie, M. Wright, J. Dubois, F. Gueritte-Voegelein, D. Guenard, R. C. Donehower, E. K. Rowinsky, *J. Natl. Cancer Inst. Monogr.* **1993**, *15*, 39.
[53] G. M. Thurber, K. S. Yang, T. Reiner, R. H. Kohler, P. Sorger, T. Mitchison, R. Weissleder, *Nat. Commun.* **2013**, *4*, 1504.
[54] a) I. Veilleux, J. A. Spencer, D. P. Biss, D. Cote, C. P. Lin, *IEEE J. Sel. Top. Quantum Electron.* **2008**, *14*, 10; b) K. Choe, Y. Hwang, H. Seo, P. Kim, *J. Biomed. Opt.* **2013**, *18*, 036005; c) J. Ahn, K. Choe, T. Wang, Y. Hwang, E. Song, K. H. Kim, P. Kim, *Biomed. Opt. Express* **2015**, *6*, 3963; d) H. Seo, Y. Hwang, K. Choe, P. Kim, *Biomed. Opt. Express* **2015**, *6*, 2158.
[55] M. M. Tomayko, C. P. Reynolds, *Cancer Chemother. Pharmacol.* **1989**, *24*, 148.
[56] E. Mehrara, E. Forssell-Aronsson, H. Ahlman, P. Bernhardt, *Cancer Res.* **2007**, *67*, 3970.